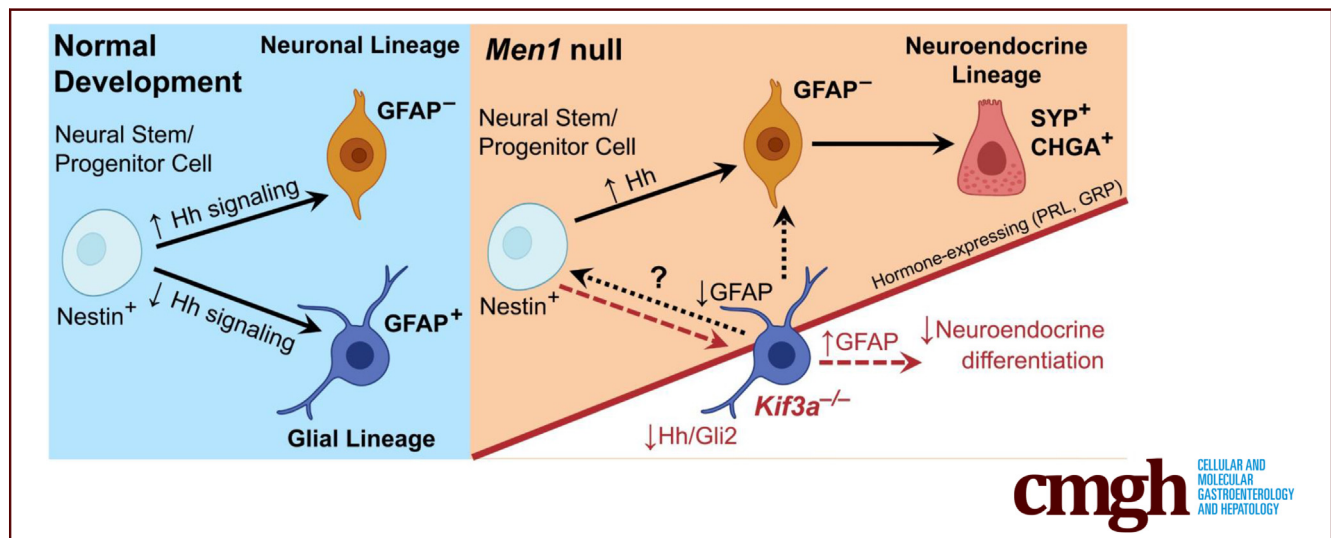


ORIGINAL RESEARCH

GFAP-directed Inactivation of *Men1* Exploits Glial Cell Plasticity in Favor of Neuroendocrine ReprogrammingSuzann Duan,¹ Travis W. Sawyer,² Ricky A. Sontz,¹ Bradley A. Wieland,¹ Andres F. Diaz,¹ and Juanita L. Merchant¹¹University of Arizona College of Medicine, Department of Medicine, Division of Gastroenterology, Tucson, Arizona; and ²Wyant College of Optical Sciences, University of Arizona, Tucson, Arizona

SUMMARY

Loss of the tumor suppressor protein menin in glial fibrillary acidic protein-expressing cells stimulates gastric neuroendocrine hyperplasia and neuroendocrine tumors in the pituitary and pancreas. Deletion of menin favors glial cell reprogramming toward a neuroendocrine phenotype with tumorigenic potential.

BACKGROUND & AIMS: Efforts to characterize the signaling mechanisms that underlie gastroenteropancreatic neoplasms (GEP-NENs) are precluded by a lack of comprehensive models that recapitulate pathogenesis. Investigation into a potential cell-of-origin for gastrin-secreting NENs revealed a non-cell autonomous role for loss of menin in neuroendocrine cell specification, resulting in an induction of gastrin in enteric glia. Here, we investigated the hypothesis that cell autonomous *Men1* inactivation in glial fibrillary acidic protein (GFAP)-expressing cells induced neuroendocrine differentiation and tumorigenesis.

METHODS: Transgenic *GFAP^{ΔMen1}* mice were generated by conditional GFAP-directed *Men1* deletion in GFAP-expressing cells. *Cre* specificity was confirmed using a tdTomato reporter. *GFAP^{ΔMen1}* mice were evaluated for GEP-NEN development and neuroendocrine cell hyperplasia. Small interfering

RNA-mediated *Men1* silencing in a rat enteric glial cell line was performed in parallel.

RESULTS: *GFAP^{ΔMen1}* mice developed pancreatic NENs, in addition to pituitary prolactinomas that phenocopied the human MEN1 syndrome. *GFAP^{ΔMen1}* mice exhibited gastric neuroendocrine hyperplasia that coincided with a significant loss of GFAP expression. *Men1* deletion induced loss of glial-restricted progenitor lineage markers and an increase in neuroendocrine genes, suggesting a reprogramming of GFAP⁺ cells. Deleting *Kif3a*, a mediator of Hedgehog signaling, in GFAP-expressing cells attenuated neuroendocrine hyperplasia by restricting the neuroendocrine cell fate. Similar results in the pancreas were observed when *Sox10* was used to delete *Men1*.

CONCLUSIONS: GFAP-directed *Men1* inactivation exploits glial cell plasticity in favor of neuroendocrine differentiation. (*Cell Mol Gastroenterol Hepatol* 2022;14:1025–1051; <https://doi.org/10.1016/j.jcmgh.2022.06.009>)

Keywords: Enteric Glia; Gastrinomas; Hedgehog Signaling; KIF3A; Primary Cilia; SOX10.

Gastroenteropancreatic neuroendocrine neoplasms (GEP-NENs) comprise a heterogeneous group of malignancies showing an increase in incidence and

prevalence across the United States.^{1,2} GEP-NENs are comprised of hormone-producing cells and include gastric carcinoids, gastrinomas, and pancreatic neuroendocrine tumors (NETs).³ The development of GEP-NENs is associated with sporadic and inherited mutations in the Multiple Endocrine Neoplasia I (*MEN1*) gene.⁴ Inactivation of the *MEN1* locus causes loss of the tumor suppressor protein menin and coincides with the development of endocrine tumors in the pancreas, pituitary, and upper gastrointestinal (GI) tract.⁵ Patients carrying a *MEN1* mutation are predisposed to developing gastrinomas, a GI NET that produces excess levels of gastrin, a peptide hormone that stimulates acid secretion and parietal and enterochromaffin cell hyperplasia.^{6–9} Such *MEN1*-associated gastrinomas preferentially develop in Brunner's glands (BGs) located within the duodenal submucosa, with an estimated >50% frequency of *MEN1* gastrinomas exhibiting lymph node metastases at the time of diagnosis.^{10,11}

Loss of menin function is a critical event underlying the formation of *MEN1* gastrinomas; however, the signaling cues that regulate menin-mediated suppression of gastrin remain elusive. Homozygous deletion of *Men1* *in utero* is embryonic lethal in mice, whereas heterozygous inactivation promotes endocrine tumors of the pancreas and pituitary, but not in the luminal GI tract.¹² Importantly, these studies did not identify potential cells-of-origin for tumor development. Subsequently, we reported the development of the first genetically engineered mouse model that displays gastric NETs.¹³ Conditional deletion of *Men1* from the GI tract epithelium using the *Villin Cre* transgene on a somatostatin-null genetic background resulted in antral G cell hyperplasia, hypergastrinemia, and gastric NETs.¹³ Systemic gastric acid suppression using a proton pump inhibitor accelerated gastric NET development and coincided with the emergence of hyperplastic gastrin-expressing enteric glial cells marked by glial fibrillary acid protein (GFAP) expression.¹⁴ The plasticity of glial cells directed towards an endocrine phenotype coincided with a reversible and non-cell autonomous loss of menin.¹⁴ Taken together, these observations suggest that hyperplastic G-cells might emerge from reprogrammed neural crest-derived cells in addition to endoderm-derived enteroendocrine cells. Indeed, prior studies have shown that multipotent glial cells marked by GFAP or SRY-box transcription factor 10 (SOX10) can generate neuroendocrine cells during normal development¹⁵ and upon overexpression of oncogenes such as *MYCN*.¹⁶ Therefore, we tested the hypothesis that cell autonomous deletion of *Men1* in GFAP-expressing cells promotes neuroendocrine cell development. Here, we show that conditional deletion of *Men1* in GFAP-expressing glial cells results in NET development in the pituitary and pancreas, in addition to neuroendocrine hyperplasia in the stomach. These events coincided with loss of the GFAP-restricted lineage and emergence of an endocrine phenotype with tissue-specific hormone expression, suggesting a direct role for glial cell reprogramming upon removal of menin. Directing *Men1* deletion to SOX10-expressing cells recapitulated pancreatic NET development and gastric neuroendocrine hyperplasia,


further supporting the premise that a neural crest-derived cell might be a cell-of-origin for GI NETs.

Results

GFAP^{ΔMen1} Mice Develop Pancreatic Neuroendocrine Neoplasms (PNETs)

To determine whether loss of menin in GFAP-expressing cells was sufficient to drive the development of GEP-NENs, we conditionally deleted *Men1* under the control of 2.2 kb of the human GFAP promoter (*GFAP^{ΔMen1}*).^{17,18} Human GFAP expression is restricted to cell types known to express GFAP, including enteric glial cells.¹⁹ Moreover, the specificity of GFAP for marking the glial lineage has been extensively reported previously.^{20–22} After 15 to 24 months of age, 11 of 22 *GFAP^{ΔMen1}* mice developed macroscopic tumors throughout the pancreas (Table 1). Histological analysis of the pancreas identified significant islet hyperplasia and features characteristic of neuroendocrine neoplasms (Figure 1, A). Pancreatic lesions varied from poorly differentiated with a solid sheet-like morphology to highly differentiated with a rosette pattern (Figure 1, B–D). Consistent with their unique histology, highly differentiated neoplasms exhibited cytoplasmic or absent menin expression (Figure 1, E) and strong immunoreactivity for the neuroendocrine markers synaptophysin (SYP) and chromogranin A (CHGA) (Figure 1, E–F). In contrast, poorly differentiated tumors were negative for CHGA and exhibited low expression of SYP (Figure 1, G). To assess whether these tumors were indeed of pancreatic islet origin, we examined the expression of iroquois homeobox protein 2 (IRX-2), a tissue-restricted transcription factor required for alpha cell lineage specification.²³ Both well-differentiated and poorly differentiated tumors exhibited strong nuclear expression of IRX-2, confirming an endocrine cell origin for both tumor types (Figure 1, F–G). Based on the proliferative index used to categorize human pancreatic NENs,²⁴ we stained *GFAP^{ΔMen1}* neoplasms for Ki-67 and classified the neoplasms as pancreatic neuroendocrine tumors (PNETs) (<2% Ki-67⁺ cells per high power field, HPF) (Figure 1, H–I) or

Abbreviations used in this paper: ACTH, adrenocorticotropic hormone; BG, Brunner's glands; BSA, bovine serum albumin; CHGA, chromogranin A; DEG, differently expressed genes; EGC, enteric glial cells; ELISA, enzyme-linked immunosorbent assay; FBS, fetal bovine serum; GCG, glucagon; GEP-NENs, gastroenteropancreatic neuroendocrine neoplasms; GFAP, glial fibrillary acidic protein; GH, growth hormone; GI, gastrointestinal; GRP, gastrin-releasing peptide; HPF, high power field; HRP, horseradish peroxidase; INS1, insulin; IRX2, iroquois homeobox protein 2; MEN1, multiple endocrine neoplasia 1; NET, neuroendocrine tumors; NF-H, neurofilament-H; OCT, optimal cutting temperature; PBS, phosphate buffered saline; pitNET, pituitary neuroendocrine tumor; PNEC, pancreatic neuroendocrine carcinoma; PNET, pancreatic neuroendocrine tumor; qPCR, quantitative polymerase chain reaction; RT, room temperature; SHH, sonic hedgehog; siRNA, small interfering RNA; SOX10, SRY-box transcription factor 10; SST, somatostatin; SYP, synaptophysin; VIP, vasoactive intestinal peptide; WT, wild-type.

 Most current article

© 2022 The Authors. Published by Elsevier Inc. on behalf of the AGA Institute. This is an open access article under the CC BY-NC-ND license (<http://creativecommons.org/licenses/by-nc-nd/4.0/>).

2352-345X

<https://doi.org/10.1016/j.jcmgh.2022.06.009>

Table 1. Summary of Phenotypes Observed in *GFAP Cre; Men1^{FL/FL}* Mice Aged 13 to 24 Months

Men1	Pancreatic hyperplasia/tumor, n/N; average age	Pituitary adenoma, n/N	Antral hyperplasia/tumor, n/N	BG/duodenal polyp, n/N	SI lipoma, n/N
WT	0/30; 17.5 mo	0/30	0/30	0/30	0/30
FL/+	1/9; 17.9 mo	1/9	1/9	1/9	0/9
FL/FL	11/36; 17.9 mo 11/22; 15 mo and older • 7/13 female • 4/9 male 0/14; Under 14 mo	18/39 • 17/30 female • 1/9 male	11/36 • 8/27 female • 3/9 male	2/36 • 2/27 female	2/36 • 2/27 female

BG, Brunner's glands; SI, small intestinal; WT, wild-type.

pancreatic neuroendocrine carcinomas (PNECs) (>20% Ki-67⁺ cells per HPF) (Figure 1, J). Classification of the Ki-67^{HIGH}/CHGA^{NEG}/SYP^{LOW} neoplasms as PNECs is consistent with human NECs exhibiting reduced expression of the classical neuroendocrine biomarkers.^{25,26} Further characterization of highly differentiated PNETs revealed the presence of both hyperplastic INS1 (insulin)-expressing beta-cells and glucagon (GCG)-expressing alpha-cells (Figure 1, K–M). Consistent with positive staining for neuroendocrine markers, PNETs exhibited a 10-fold increase in *Chga* transcript and a trending but nonsignificant increase in *Syp* mRNA expression compared with normal pancreas (Figure 1, N).

PNETs were predominantly comprised of PNETs (approximately 83% of all PNET-bearing mice), whereas PNECs were only observed in 2 mice (comprising 17% of all PNET-bearing mice, one of which was heterozygous for *Men1* deletion). Notably, there was not a mixture of NETs and NECs in the same mice. As gender-related differences have been previously reported in patients with MEN1 syndrome,^{27,28} we further stratified the occurrence of *GFAP^{ΔMen1}* PNECs and PNETs by sex (Table 1; Figure 1, O). Both cases of PNECs occurred in female mice. The incidence of PNETs was slightly higher in female mice compared with male mice, occurring in 7 of 13 females vs 4 of 9 males over the age of 15 months (53% vs 44%, respectively). Interestingly, female *GFAP^{ΔMen1}* mice tended to present with multiple lesions compared with males that presented with a solitary tumor (Figure 1, P). Of the 7 female tumor-bearing mice, 6 (86%) had 2 or more PNETs compared with only 1 of 4 (25%) males. As anticipated, *GFAP^{ΔMen1}* mice exhibited significantly elevated levels of circulating GCG and INS1 hormones, with tumor-bearing mice generally exhibiting the highest hormone expression irrespective of sex (Figure 1, Q–R). Consistent with the opposing effects of GCG and INS1 on glucose regulation, serum glucose levels were unchanged in *GFAP^{ΔMen1}* mice regardless of sex and tumor status (Figure 1, S).

Development of PNETs in *GFAP^{ΔMen1}* Mice Coincides With Loss of GFAP Expression

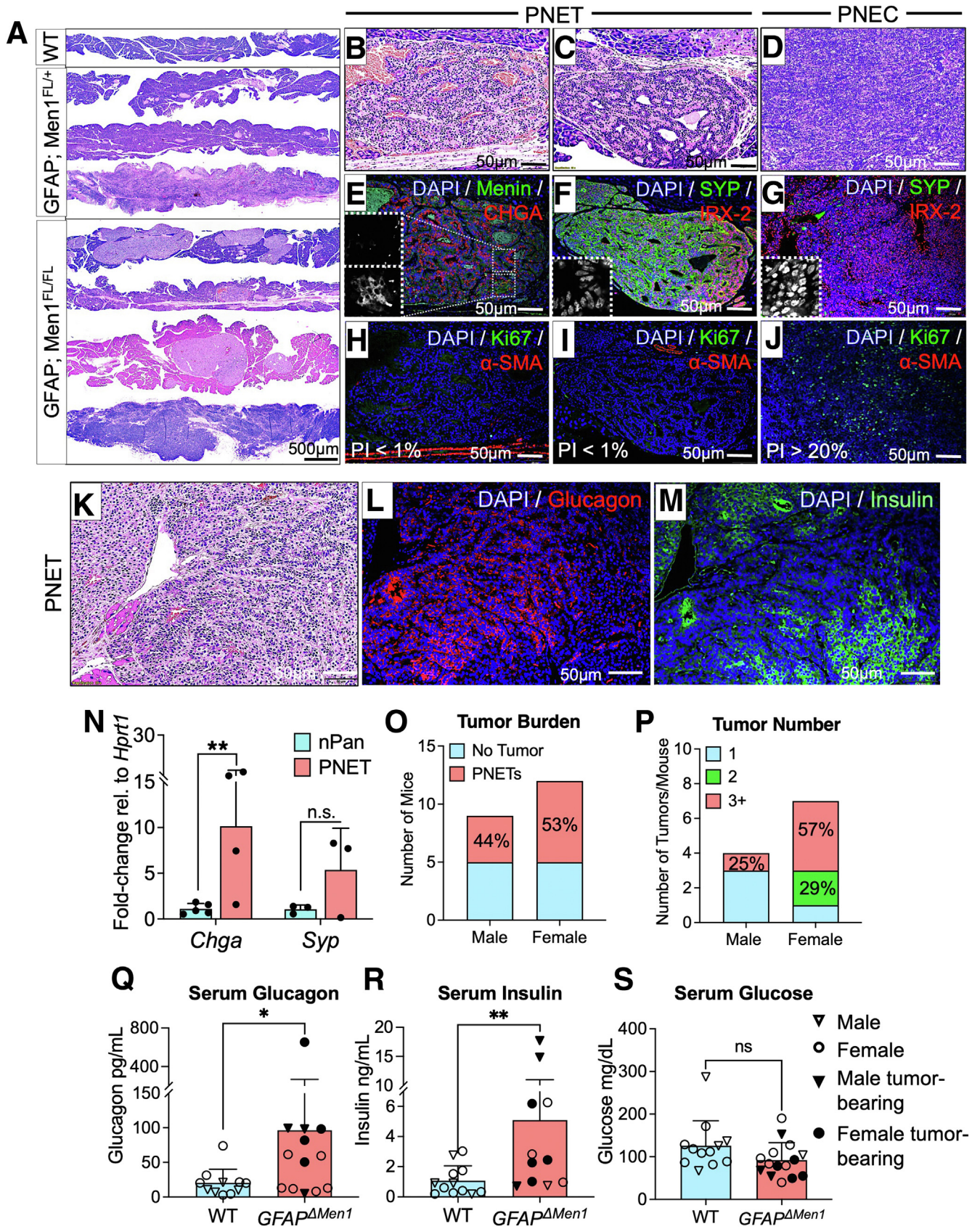
Due to the low overall incidence of PNECs, we focused our subsequent investigation on PNETs only. To determine

the effect of *Men1* loss on GFAP expression in PNETs, we stained normal pancreas and PNETs for GFAP. Consistent with previous reports, GFAP expression was strongly localized to the periphery of SYP⁺ and hormone-expressing islets in both wild-type and *GFAP^{ΔMen1}* mice;²⁹ however, GFAP expression was uniquely lost in cells encircling the PNETs (Figure 2, A–B). Consistent with this loss, the expression of glial lineage transcripts *Gfap* and *S100b* were significantly lower in PNETs compared with the pancreas of wild-type (WT) mice, whereas *Men1* mRNA exhibited a trending decrease (Figure 2, C). The specificity of GFAP marking the glial lineage was confirmed by showing that GFAP did not colocalize with phospho-Neurofilament-H (NF-H)-expressing nerve fibers in the pancreas and in PNETs (Figure 2, A–B). To further evaluate the specificity of *GFAP Cre* expression, we generated *GFAP Cre-loxP-tdTomato* mice and confirmed that fluorescent tdTomato protein expression associated with GFAP and the glial lineage markers S100B and p75^{NTR} in frozen mouse pancreas sections, as previously reported¹⁹ (Figure 2, D–E). As expected, GFAP-tdTomato expression did not co-localize with NF-H⁺ nerve fibers, further confirming the specificity of GFAP marking the glial lineage. In summary, development of well-differentiated PNETs in this model coincided with loss of GFAP expression from the periphery of normal pancreatic islets.

We next evaluated whether *GFAP^{ΔMen1}* PNETs carried the potential to propagate in 3-D organoid culture as a measure of stemness. Organoid lines were established from PNETs from 4 mice and cultured for 3 weeks prior to staining or cryopreservation (Figure 2, F). Similar to parent tumors, the organoids strongly expressed SYP, CHGA, GCG, and INS1, but only a few cells exhibited Ki-67 positivity (Figure 2, F). Therefore, PNET-derived organoids recapitulated the biological features of their parent tumors and exhibited stem-like features in the absence of Ki-67 expression.

GFAP^{ΔMen1} Mice Develop PitNETs That Phenocopy Human MEN1 Prolactinomas

Nine of 30 female *GFAP^{ΔMen1}* mice presented with clinical signs of hydrocephalus starting at 15 months of age, including presentation of a domed head appearance, loss of



muscle coordination, seizures, and repetitive motor movements. Following the onset of hydrocephalus, mice were necropsied, and brains were analyzed for potential effects of GFAP-directed *Men1* inactivation. The overarching rationale for these studies was emphasized by the fact that GFAP is the main intermediate filament protein in brain astrocytes and other cells of the glial-restricted lineage.³⁰ We discovered that *GFAP^{ΔMen1}* mice developed hemorrhagic pituitary adenomas (Figure 3, A–B). Subsequent immunostaining of *GFAP^{ΔMen1}* adenomas demonstrated diffuse immunoreactivity for SYP and CHGA as expected (Figure 3, C). Strong staining for prolactin showed these tumors to be prolactinomas (Figure 3, D). As prolactin is produced by lactotropes of the PIT-1⁺ lineage, we stained pituitary NETs for the cell-patterning transcription factor PIT-1. As expected, tumors exhibited strong expression of PIT-1, thus confirming that both pancreatic and pituitary NETs arise in the context of endocrine lineage-specific transcription factor expression (Figure 3, E). Additionally, Ki-67 inversely correlated with the expression of neuroendocrine markers, with stronger neuroendocrine status associated with lower Ki-67 staining (Figure 3, E). Because cells of the PIT-1⁺ lineage also comprise growth hormone (GH)-expressing somatotrophs but not adrenocorticotrophic hormone (ACTH)-expressing corticotrophs,³¹ we stained pituitary tumors for GH and ACTH expression. Tumors exhibited patchy but generally robust expression of GH, whereas the expression of ACTH was restricted to only a few cells (Figure 3, F). These observations were consistent with the fact that pituitary tumors arising in the human MEN1 syndrome are most commonly comprised of prolactinomas and pluri-hormone-secreting adenomas (ie, secreting prolactin and a second hormone), with growth hormone-producing tumors being the next most common tumor type.^{27,32}

Similar to previous reports of gender differences in human MEN1 patients, the emergence of pituitary tumors in mice was strikingly sex-dependent.^{27,28,33} Female *GFAP^{ΔMen1}* mice (17 of 30; 57%) developed macroscopic pituitary adenomas as early as 15 months of age, whereas only 1 of 9 males (11%) developed a pituitary tumor (Table 1; Figure 3, G). Consistent with tumors staining strongly for prolactin, *GFAP^{ΔMen1}* mice exhibited significantly higher serum prolactin levels compared with age-matched littermate controls (Figure 3, H). Neuroendocrine transcripts *Chgb*, *Syp*, and *Enolase 2* (*Eno2*) were significantly elevated in *GFAP^{ΔMen1}* pitNETs compared with WT pituitary. Moreover, mRNA levels of *prolactin* and *vasoactive*

intestinal peptide (*Vip*) hormones were 15-fold higher in pitNETs compared with normal pituitary (Figure 3, I). Further evaluation of GFAP and menin expression in *GFAP^{ΔMen1}* prolactinomas showed absent GFAP staining and low expression of menin within the tumor compared with the adjacent hypothalamus (Figure 3, J). Similar to the previous observations in PNETs, *Gfap* and *Men1* mRNA expression was significantly reduced in prolactinomas compared with WT pituitary (Figure 3, K).

Because GFAP marks nestin⁺ subventricular neural stem cells^{34–36} and interacts with menin,^{37,38} we determined whether GFAP-negative *GFAP^{ΔMen1}* pitNETs share features with neural stem cells by generating tumor neurosphere lines from multiple *GFAP^{ΔMen1}* pituitary prolactinomas. Subsequent immunostaining of *GFAP^{ΔMen1}* tumor neurospheres revealed that tumor cells co-expressed prolactin and the neural stem cell markers SOX2 and nestin, suggesting that the hormone-expressing tumor cells arose from a neural stem cell lineage (Figure 3, L). Positive SOX2⁺ expression in tumor neurospheres was consistent with strong SOX2-immunoreactivity in parent pitNETs (Figure 3, M). Thus, like PNETs that carried the potential to propagate as organoids, pitNETs also exhibited features of stemness that allowed them to be subcultured as 3-D neurospheres.

Hyperplastic Reprogramming of the GI Epithelium in *GFAP^{ΔMen1}* Mice

To determine whether loss of menin in enteric GFAP-expressing cells supports the development of NENs in the luminal GI tract, we evaluated the stomach and proximal small intestine of *GFAP^{ΔMen1}* mice for changes in enteroendocrine cell numbers and composition. Although no gastrinomas or small intestinal NENs were observed at 14 to 24 months of age, 11/36 *GFAP^{ΔMen1}* mice (30%) showed hyperplastic changes in the proximal and distal stomach (Table 1; Figure 4, A). We further observed the development of small intestinal lipomas and duodenal polyps emerging from the BGs at a low incidence (2/36 mice; 5%). In contrast to the previous observations of sex differences in the occurrence of NETs, the incidence of gastric hyperplasia was similar between male and female mice (33% and 30%, respectively) (Figure 4, A).

Compared with WT mice, *GFAP^{ΔMen1}* mice exhibited histological evidence of hyperplasia and metaplasia marked by parietal cell atrophy (Figure 4, B–C). These events coincided with increased expression of CHGA and SYP in the corpus, and CHGA, SYP, and gastrin in the gastric antrum. Notably, CHGA and SYP

Figure 1. (See previous page). **GFAP-directed inactivation of *Men1* promotes pancreatic islet hyperplasia and the development of pancreatic neuroendocrine neoplasms.** (A) Hematoxylin and eosin (H&E) stains of well differentiated and poorly differentiated tumors in *GFAP^{ΔMen1}* mice compared with WT and heterozygous groups. (B–C) H&E stains of well differentiated *GFAP^{ΔMen1}* PNETs compared with a poorly differentiated PNEC (D). (E) Immunofluorescent staining of a PNET for CHGA and menin. *Insets*: representative images of a PNET showing absent or cytoplasmic menin in the tumor (*white*). Immunofluorescent staining of a PNET (F) and PNEC (G) for SYP and the alpha cell-specification factor IRX-2. *Insets*: IRX-2 is expressed in the nucleus of tumor cells (*white*). (H–I) Ki-67 and smooth muscle actin (SMA) staining of PNETs compared with a PNEC (J). Proliferative index (PI) is indicated by the percentage of Ki67-positive tumor cells in each HPF. K) H&E stain of a *GFAP^{ΔMen1}* PNET stained for GCG (L) and INS1 (M). (N) Quantitation of *Chga* and *Syp* mRNA in WT pancreas and *GFAP^{ΔMen1}* PNETs. N = 3–5 mice per group; **P < .01. Data are represented as mean ± standard deviation. (O) Number of mice presenting with pancreatic neuroendocrine neoplasms as stratified by sex. (P) Number of PNETs per mouse in males vs females. Levels of GCG (Q) INS1 (R) and glucose (S) in sera of WT and *GFAP^{ΔMen1}* mice, with symbols indicating male or female mice with and without tumors. N = 11–12 mice per group; *P < .05; **P < .01. Data are represented as mean ± standard deviation.

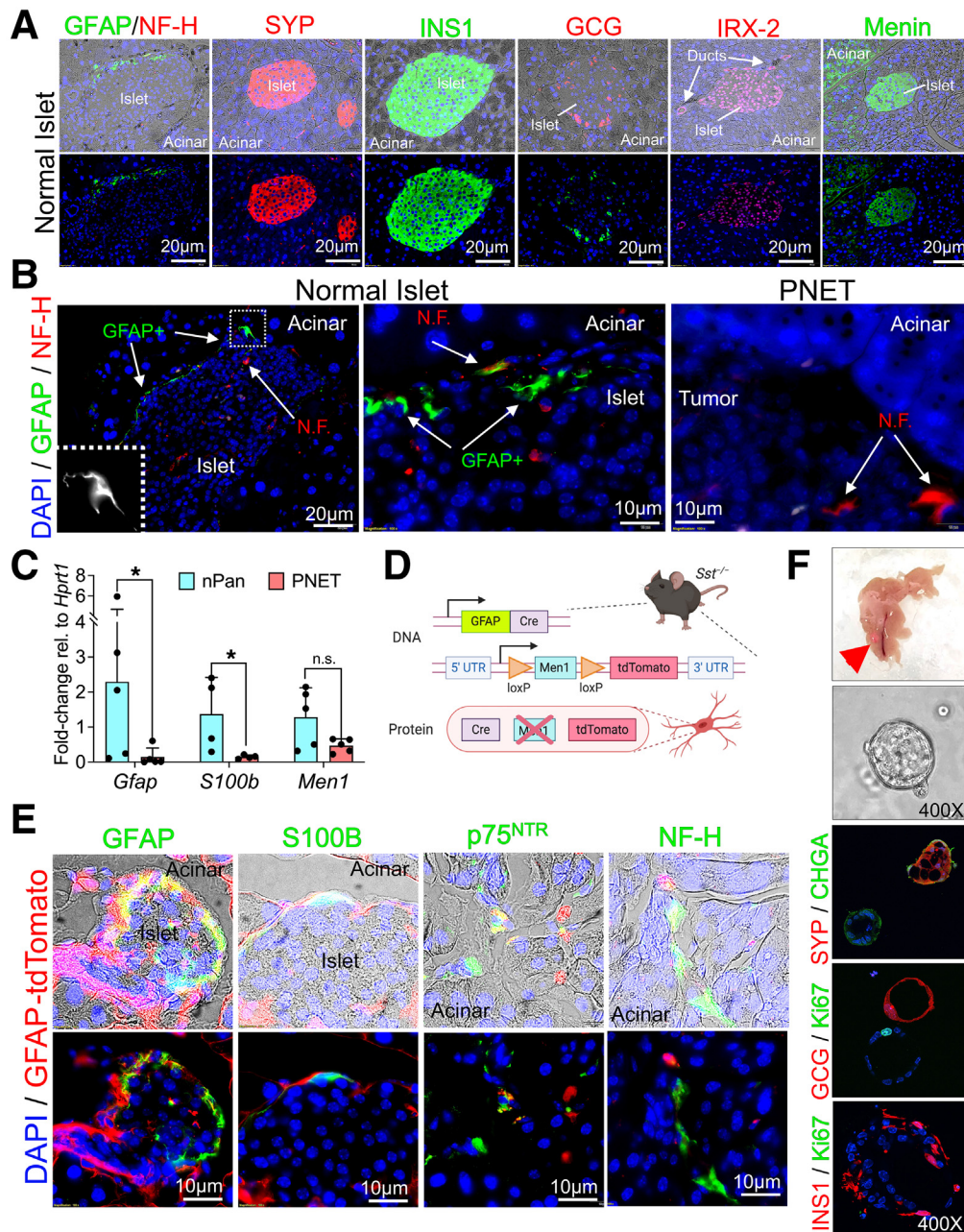


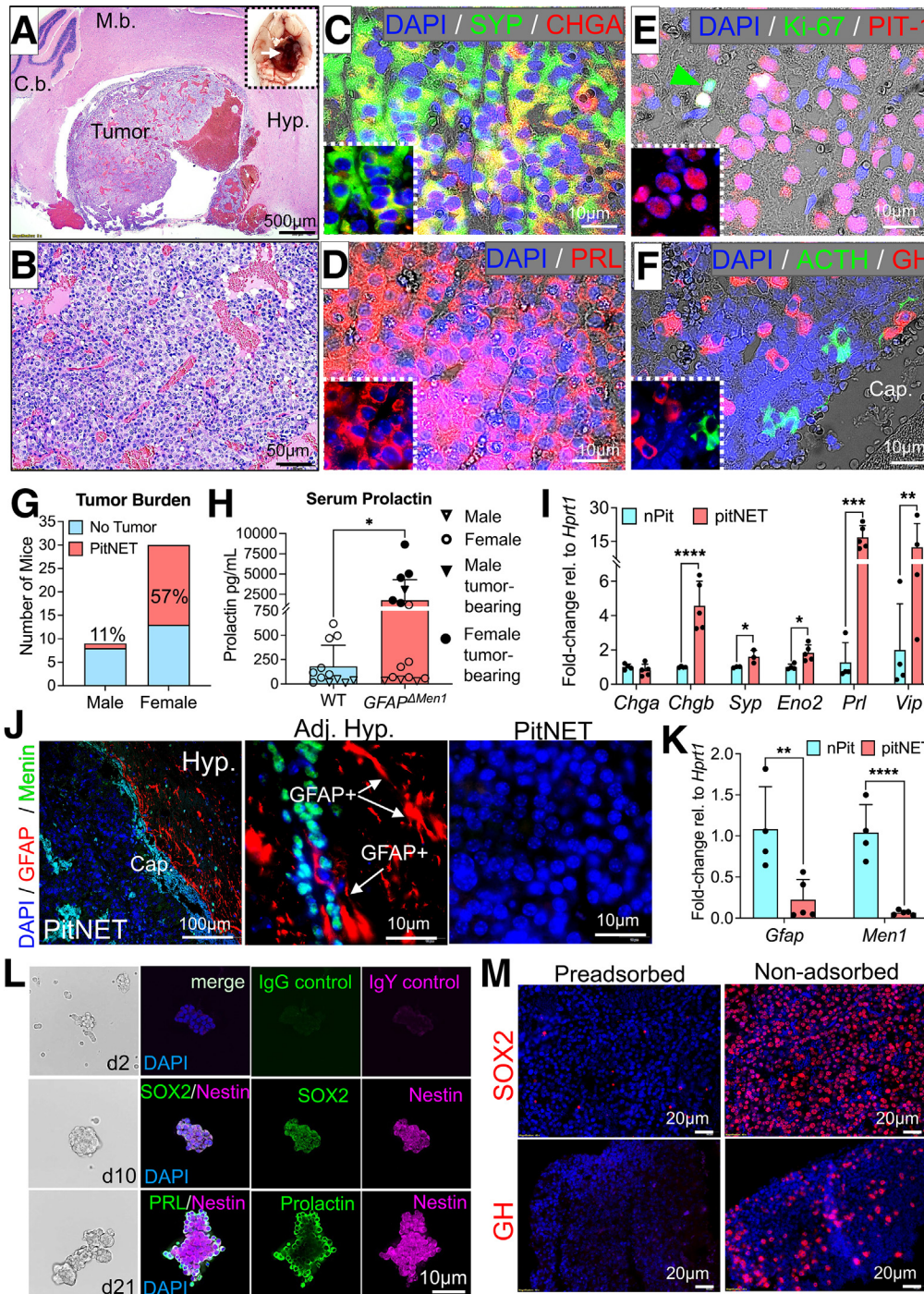
Figure 2. *GFAP*^{Δ*Men1*} PNETs exhibit loss of GFAP expression and maintain stemness in 3D culture. (A) Immunofluorescent staining of a WT mouse pancreatic islet for the glial-restricted progenitor lineage marker GFAP, the nerve fiber marker NF-H, SYP, the beta-cell hormone INS1, the alpha-cell markers GCG and IRX-2, and menin. (B) Representative images of a normal islet and *GFAP*^{Δ*Men1*} PNET stained for GFAP in green and the nerve fiber marker NF-H in red, indicating the absence of GFAP expression in and surrounding the PNET. (C) Quantitation of *Gfap*, *S100b* and *Men1* mRNA in WT pancreas and *GFAP*^{Δ*Men1*} PNETs. N = 4–5 mice per group; **P* < .05; ***P* < .01. Data are represented as mean ± standard deviation. (D) Schematic of *GFAP*^{Δ*Men1*}-tdTomato construct for endogenous labeling of GFAP. (E) Immunofluorescent images of frozen pancreas sections from WT *GFAP*-tdTomato mice co-stained for the glial-restricted progenitor lineage markers GFAP, S100B, and P75^{NTR}, in addition to NF-H as a negative marker for the glial lineage. Immunofluorescent images were merged on a transmitted light micrograph to distinguish islets from acinar cells. (F) Top to bottom: Macroscopic image of a *GFAP*^{Δ*Men1*} pancreas, with an arrow indicating the presence of a PNET and phase contrast image of a corresponding PNET organoid. PNET organoids were stained for CHGA, SYP, GCG, INS1, and Ki-67 and imaged by confocal microscopy. Images are representative of PNET organoids derived from 4 tumor-bearing mice (n = 4).

did not co-localize in all cells of the proximal and distal stomach, suggesting the presence of divergent endocrine cell populations. Whereas all gastrin⁺ cells appeared to express SYP, not all G cells expressed CHGA (Figure 4, C). Increased

expression of *Chga*, *Syp*, and *Gast* mRNA was confirmed by quantitative polymerase chain reaction (qPCR), and this was consistent with increased numbers of CHGA⁺, SYP⁺, and gastrin⁺ cells in the gastric antra of *GFAP*^{Δ*Men1*} mice

(Figure 4, D–E). No differences in endocrine mRNA levels were observed in the proximal duodenum, indicating that hyperplastic reprogramming of endocrine cells was limited to the stomach. Consistent with increased G cell numbers and tissue gastrin expression, *GFAP^{ΔMen1}* mice exhibited a small but significant increase in serum gastrin levels compared with littermate controls (Figure 4, F). Previous studies in transgenic mice identified hypergastrinemia-induced changes to the gastric epithelium, including parietal cell atrophy.^{39,40} Here, we also observed decreased gastric acid levels in the setting of hypergastrinemia in *GFAP^{ΔMen1}* mice,

consistent with the presence of metaplasia (Figure 4, G). qPCR analysis of other gastric cell types further confirmed decreased expression of the parietal cell-specific marker *Atp4b* and significant upregulation of *Gif*, a marker of zymogenic chief cells (Figure 4, H–I). Therefore, conditional deletion of menin in enteric GFAP-expressing cells stimulated neuroendocrine hyperplasia that is specific to the corpus and gastric antrum. However, unlike the pancreatic islets and pituitary, glial-directed *Men1* deletion was insufficient to convert the hyperplastic endocrine cells into NETs.



Loss of *Men1* Reduces GFAP Expression in GFAP^{ΔMen1} Mice and In Vitro

Because NET development in the pituitary and pancreas coincided with loss of GFAP expression, we examined the impact of *Men1* deletion on the fate of GFAP-expressing cells in vivo. We performed fluorescent imaging of both whole tissue mounts and frozen sections of *GFAP Cre*-tdTomato mice to confirm the specificity of *GFAP Cre* expression throughout the stomach (Figure 5, A–B). Consistent with previous characterization of this model,¹⁹ fluorescent tdTomato protein expression was strongly localized to the myenteric plexus in whole tissue mounts (Figure 5, A). Further, tdTomato expression co-localized at the cellular level with GFAP protein and the glial lineage markers S100B and p75^{NTR}, but not with NF-H⁺ nerve fibers, as expected (Figure 5, B). Surprisingly, ex vivo fluorescent imaging of tissues from *GFAP^{ΔMen1}* mice revealed a ~4-fold reduction in the tdTomato signal across the upper GI tract compared with wild-type mice (Figure 5, C–D). Imaging of frozen tissue sections confirmed near-loss of tdTomato fluorescence in the mucosa and lamina propria, whereas some signal was still retained in the submucosal and myenteric plexi (Figure 5, E). Therefore, deletion of *Men1* in GFAP⁺ cells extinguished GFAP expression.

A prior study showed that GFAP and menin proteins interact in astrocytes, suggesting that the 2 proteins might be interdependent.³⁷ To test whether this interaction also occurs in GFAP-expressing glial cells, we performed co-immunoprecipitation using cytoplasmic extracts from a rat enteric glial cell line (EGC) and confirmed interaction between GFAP isoforms and menin (Figure 4, F–G). Studies were performed in EGCs as they are known to express GFAP and menin, and these cells also exhibit robust growth in culture compared with primary glial cells. To test whether loss of menin in a GFAP-expressing cell type modulates the expression of GFAP, we used small interfering RNA (siRNA) to knockdown *Men1* expression in GFAP⁺ EGCs. Consistent with the in vivo observations, *Men1* silencing decreased the expression of GFAP and S100B at the transcript and protein

levels (Figure 5, H–J). Taken together, these results indicated a role for menin in regulating glial cell identity by modulating GFAP expression.

Transcriptome-wide Analysis of Gastric Neuroendocrine Hyperplasia and Pituitary NETs Supports Glial-to-neuroendocrine Reprogramming

Because GFAP-specific deletion of menin was sufficient to drive NET formation in the pituitary and pancreas but not in the stomach or intestine, we used RNA-Seq to identify the molecular pathways that might contribute to the transition from neuroendocrine hyperplasia to NET development. *GFAP^{ΔMen1}* pitNETs, gastric antrum, and their respective WT counterparts were submitted for bulk RNA sequencing. Unsurprisingly, the number of significant differentially expressed genes (DEGs) was 10 times higher when comparing normal pituitary with pitNETs vs the antral tissues of both genotypes (Figure 6, A–B). As expected, a number of genes related to neuroendocrine differentiation were upregulated in both datasets (eg, *Grp*, *Vip*, *Syp*, and *Ncam1/2* in antra and *Prl*, *Chgb*, *Eno2*, *Cckbr*, *Vip*, and *Ascl2* in pitNETs) (Figure 6, C–D). Genes associated with the neuroglial-restricted lineage were significantly upregulated in *GFAP^{ΔMen1}* tissues compared with WT controls (Figure 6, E). Furthermore, most upregulated antral genes were correlated with neural differentiation and acquisition of a neuronal cell fate, including *Ngfr*, *Elav3/4*, *Nrsn1/2*, *Phox2b*, *Nos1*, *Tubb3*, *Uchl1*, *Ret*, and *Hoxb* (Figure 6, E). PitNETs also exhibited increased expression of neural-specific transcripts (eg, *Elav3/4*, *Nrsn1/2*, and *Tubb3*) that coincided with significant downregulation of glial lineage-associated genes, including *Gfap* and others (Figure 6, F). Consistent with their ability to propagate in 3-D culture, pitNETs exhibited increased expression of neural crest cell transcripts related to stemness, including *Vim*, *Fabp7*, and *Sox11* (Figure 6, F).

Enteric neurons express gastrin-releasing peptide (GRP),⁴¹ which was identified in the RNA-seq dataset as the

Figure 3. (See previous page). *GFAP^{ΔMen1}* mice develop pitNETs that phenocopy human MEN1 prolactinomas. (A) Hematoxylin and eosin (H&E) image of a sagittal section of a *GFAP^{ΔMen1}* pitNET labeled with adjacent brain structures (C.b., Cerebellum; Hyp., hypothalamus; M.b., midbrain). Inset shows a representative macroscopic image of a pitNET with an arrow indicating to the tumor. (B) Higher magnification image of a pitNET showing classical “salt and pepper” nuclei characteristic of well-differentiated NETs. Immunofluorescent staining of a *GFAP^{ΔMen1}* pitNET for SYP and CHGA (C), prolactin (D), and (E) Ki-67 and the pituitary specification factor PIT-1. Green arrow indicates a single Ki-67⁺ cell in the tumor. (F) Representative immunofluorescent image of a *GFAP^{ΔMen1}* pitNET stained for the anterior pituitary hormones ACTH and GH, showing increased expression of the latter. As pitNETs were highly vascularized, immunofluorescent images were merged on a transmitted light micrograph to distinguish tumor cells from red blood cells (Cap., Capillary). (G) Number of mice presenting with pitNETs as stratified by sex. (H) Serum prolactin levels in male and female mice with or without pitNETs. N = 12–15 mice per group; *P < .05 by the unpaired Student t test. Data are represented as mean ± standard deviation. (I) Quantitation of neuroendocrine-related transcripts in WT pituitary and *GFAP^{ΔMen1}* pitNETs. N = 4–5 mice per group, with the exception of the WT pituitary group, which represents 4 samples of 3 pooled pituitaries, for a total of 12 tissues in this group; *P < .05; **P < .01; ***P < .001; ****P < .0001. (J) PitNETs show absent expression of menin and GFAP compared with the adjacent hypothalamus (Hyp). Left panel: a capillary (Cap.), characterized by auto fluorescent red blood cells, separates the 2 compartments. Middle panel: Robust GFAP staining (red) in a *GFAP^{ΔMen1}* hypothalamus with few cells co-expressing menin (green). Right panel: Tumor is negative for menin and GFAP. (K) Quantitation of *Gfap* and *Men1* mRNA in WT pituitary and *GFAP^{ΔMen1}* pitNETs. Data are represented as mean ± standard deviation. (L) Representative images of tumor neurospheres generated from 3 tumor-bearing mice (n = 3). Phase contrast images show growth at days (d) 2, 10, and 21. Tumor neurospheres were stained for prolactin (PRL) and the neural stem cell markers nestin and SOX2. (M) Specificity of select antibodies was tested by preadsorption. Immunofluorescent images of a pitNET stained with non-adsorbed and pre-adsorbed GH and SOX2 antibodies.

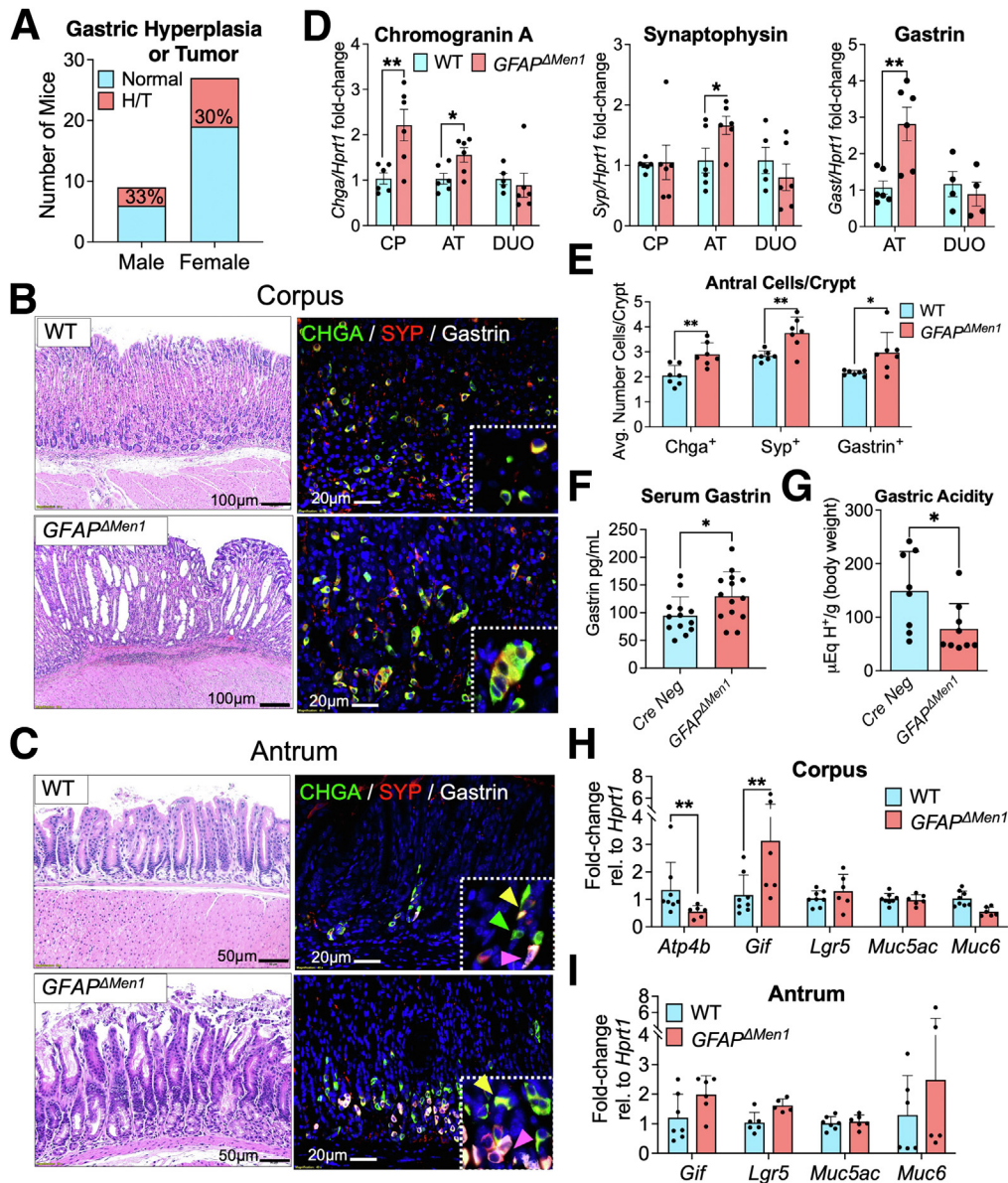


Figure 4. GFAP-directed deletion of *Men1* stimulates hyperplastic reprogramming of the gastro-intestinal epithelium and promotes neuroendocrine cell hyperplasia. (A) Number of mice presenting with gastric hyperplasia and antral tumors, as stratified by sex. (B) Representative hematoxylin and eosin (H&E) and immunofluorescent images of WT and *GFAP^{ΔMen1}* corpus stained for CHGA, SYP, and gastrin. Bottom H&E indicates parietal cell atrophy consistent with metaplasia. (C) Representative H&E and immunofluorescent images of WT and *GFAP^{ΔMen1}* gastric antrum showing increased numbers of CHGA- (green), SYP- (red), and gastrin- (white) positive cells. Colored arrows indicate the degree of co-localization amongst the 3 markers: yellow indicates cells where all 3 markers are expressed, whereas magenta indicates cells expressing gastrin and SYN only. (D) Expression of *Chga*, *Syp*, and *Gast* mRNA in WT and *GFAP^{ΔMen1}* corpus (CP), gastric antrum (AT), and duodenal mucosa (DUO). N = 6 mice per group; **P* < .05; ***P* < .01. (E) Average number of CHGA-, SYP-, and gastrin-positive cells per crypt counted across three 400× fields in the mid-antrum. N = 7 mice per group. **P* < .05 by 2-way analysis of variance. (F) *GFAP^{ΔMen1}* mice exhibit elevated serum gastrin levels compared with WT littermates. N = 12–15 mice per group; **P* < .05 by unpaired *t* test. (G) Evaluation of gastric acidity in *GFAP^{ΔMen1}* mice and controls. N = 8–9 mice per group. **P* < .05 by unpaired *t* test. The expression of non-enteroendocrine cell transcripts was evaluated in the corpus (H) and gastric antrum (I) of WT and *GFAP^{ΔMen1}* mice. N = 6–8 mice per group; **P* < .05; ***P* < .01 by 2-way analysis of variance. All data are represented as mean ± standard deviation.

most significantly upregulated transcript in *GFAP^{ΔMen1}* gastric antra. Increased GRP provides a direct mechanism for increased antral gastrin levels in these mice. Hence, we evaluated whether GFAP-directed deletion of *Men1* stimulates GRP expression leading to G cell expansion by staining

the gastric antra of *GFAP^{ΔMen1}* mice for GRP. As anticipated, *GFAP^{ΔMen1}* mice exhibited increased antral expression of GRP, and its expression co-localized with SYP in the epithelial mucosa but did not overlap with NF-H⁺ nerve fibers (Figure 6, G–H). The specificity of GRP antibody binding

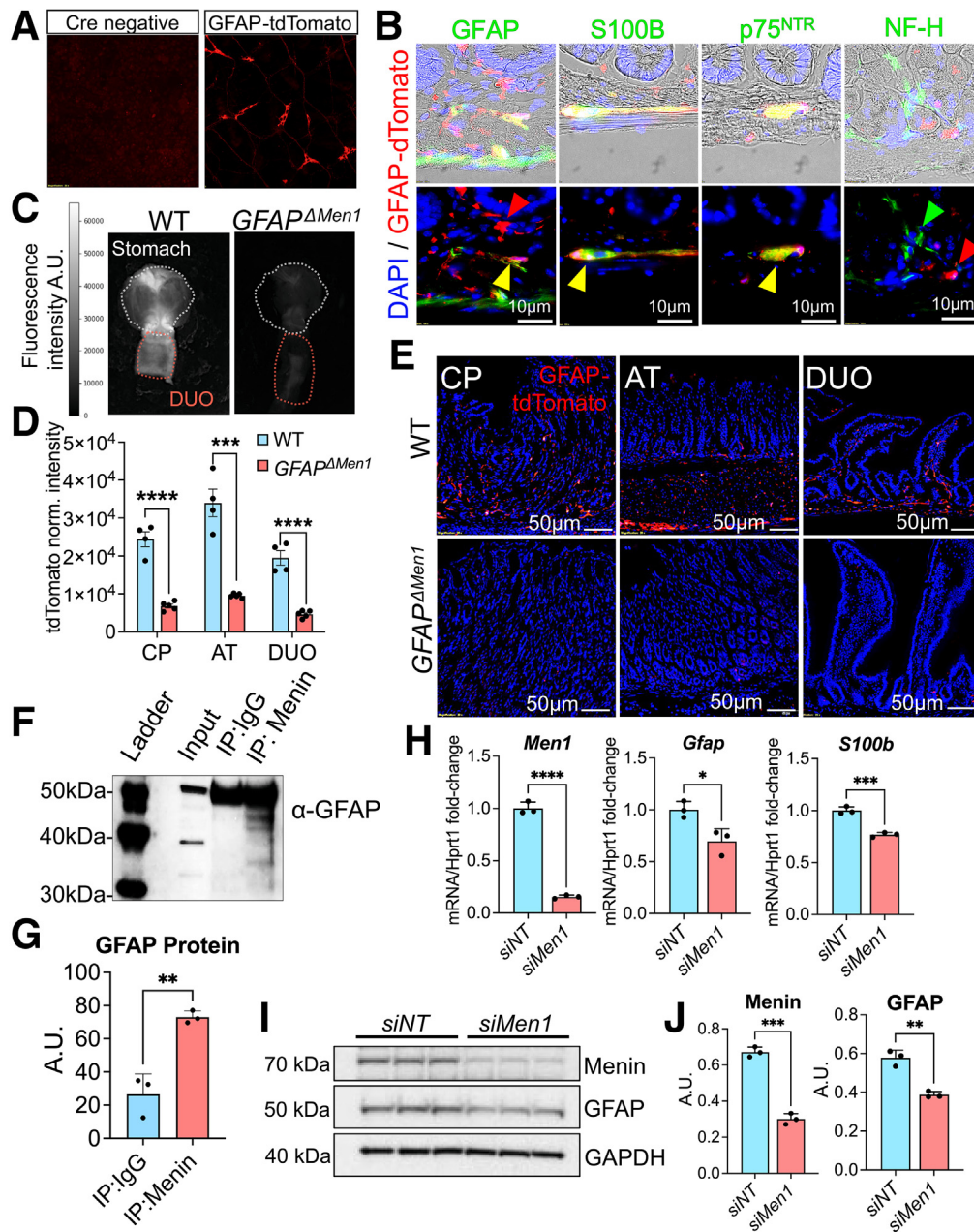
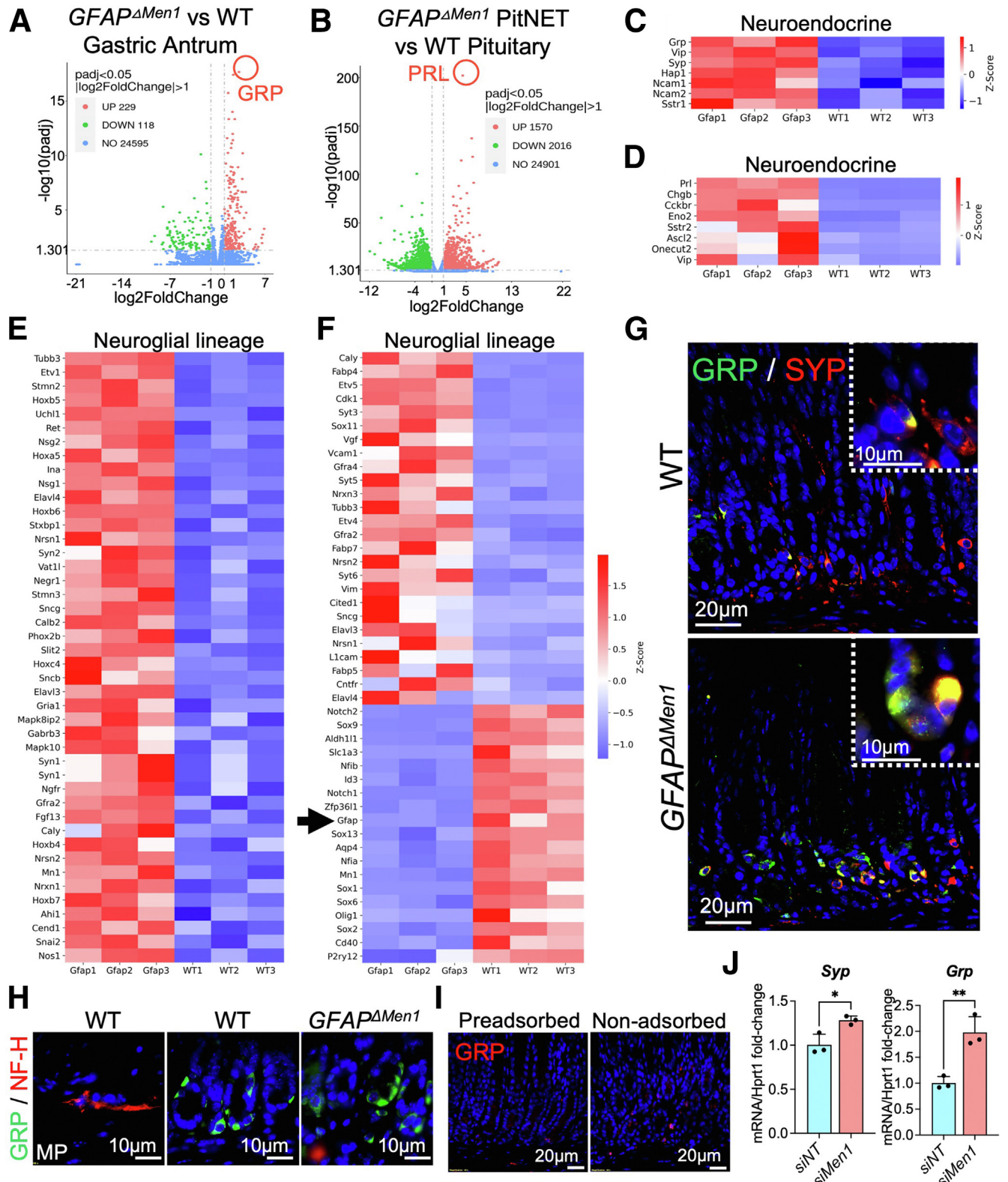


Figure 5. Conditional deletion of menin in GFAP⁺ cells stimulates reprogramming from a glial-restricted progenitor lineage. (A) Whole tissue mounts of proximal duodenum from Cre-negative and tdTomato-expressing mice showing tdTomato fluorescence localized to the myenteric plexus (MP). (B) Immunofluorescent images of frozen stomach sections from WT *GFAP*-tdTomato mice co-stained for the glial-restricted progenitor lineage markers GFAP, S100B, and p75^{NTR}, showing strong localization to the same cell types. Negative localization with the nerve fiber marker NF-H serves as a control. Immunofluorescent images were merged on a transmitted light micrograph to distinguish submucosal layers. Widefield images (C) and quantitation (D) of tdTomato signal in the stomach and duodenum of WT and *GFAP^{ΔMen1}* mice expressing tdTomato reporter. N = 4–5 mice per group; ****P* < .001; *****P* < .0001. (E) Representative images of cryosections of corpus (CP), gastric antrum (AT), and proximal duodenum (DUO) from WT and *GFAP^{ΔMen1}* mice expressing tdTomato. (F) Co-immunoprecipitation (Co-IP) of menin from rat EGC lysate followed by Western blot for GFAP. Input is 5% of lysate used for IP. (G) Quantitation of band density in 3 Co-IP experiments comparing expression of GFAP with IP with IgG isotype control in cell extracts. (H) Expression of *Men1* and the glial transcripts *Gfap* and *S100b* following siRNA-mediated *Men1* silencing in cultured rat EGCs. N = 3 independent experiments; **P* < .05; ****P* < .001; *****P* < .0001. (I) Western blot of menin and GFAP in whole cell lysates following 72-hour *Men1* silencing in rat EGCs with (J) quantitation of band density normalized to loading control. N = 3 experiments; ***P* < .01; ****P* < .001 by unpaired *t* test. All data are represented as mean ± standard deviation.

was further validated by preadsorption with recombinant GRP protein (Figure 6, I). Lastly, we assessed whether loss of menin in GFAP⁺ EGCs directly stimulates the expression of *Grp* and *Syp* to further explain a mechanism for the

induction of *Grp* and other neuroendocrine transcripts in *GFAP^{ΔMen1}* mice. Indeed, *Men1* silencing in rat EGCs induced *Grp* and *Syp* mRNA expression (Figure 6, J). Taken together, these results demonstrate that *Men1* deletion suppresses



the mature glial lineage in favor of a neuroendocrine phenotype, perhaps due to loss of GFAP.

Transcriptome Analysis Identifies Molecular Targets in Neuroendocrine Differentiation Leading to Gastric Neuroendocrine Hyperplasia and NET Development in $GFAP^{\Delta Men1}$ Mice

To further home in on the molecular changes leading to gastric neuroendocrine hyperplasia and NET development, we identified significant DEGs associated with growth and developmental pathways. Consistent with the role of menin in regulating proliferation and endocrine cell development, $GFAP^{\Delta Men1}$ pitNETs exhibited increased expression of genes involved in cell cycle inhibition, senescence, and differentiation (eg, *Cdkn1a*, *Cdkn2a*, and *Cend1*), as well as tissue development (eg, *Shh*, *Nog*, *Bmp2/7*, *Bdnf*, and *Ezh2*) (Figure 7, A–B). Increased expression of genes related to NET differentiation and cellular senescence identified by RNA-seq were further validated by qPCR of pituitary and pancreatic NETs and age-matched WT tissues (Figure 7, C–D). Datasets comparing $GFAP^{\Delta Men1}$ gastric antra and pitNETs with their respective WT tissues showed an enrichment of genes involved in neuroactive ligand receptor interaction and synaptic signaling pathways known to be upregulated in NET development (Figure 7, E–F). Interestingly, $GFAP^{\Delta Men1}$ pitNETs uniquely showed perturbations in the Hedgehog signaling pathway, which was consistent with increased expression of *Shh* mRNA and ciliary motor proteins known to facilitate transduction of Hedgehog signaling (Figure 7, B, C, and E). In contrast, increased expression of neuroendocrine and neural-lineage genes in $GFAP^{\Delta Men1}$ antral extracts coincided with downregulation of cytokeratins and immune-related transcripts marking epithelial and immune cells, respectively (Figure 7, H–I). Collectively, transcriptome-wide sequencing identified the involvement of dysregulated cell cycle and developmental pathways prefacing NET development and suggests a potential role for Hedgehog signaling in mediating the transition from neuroendocrine hyperplasia to tumorigenesis.

Impairment of Sonic Hedgehog Signaling (SHH) in Enteric $GFAP^+$ Cells Attenuated Neuroendocrine Cell Hyperplasia in $GFAP^{\Delta Men1}$ Mice

Hedgehog signaling mediated by primary cilia is known to promote premature differentiation of neural progenitor

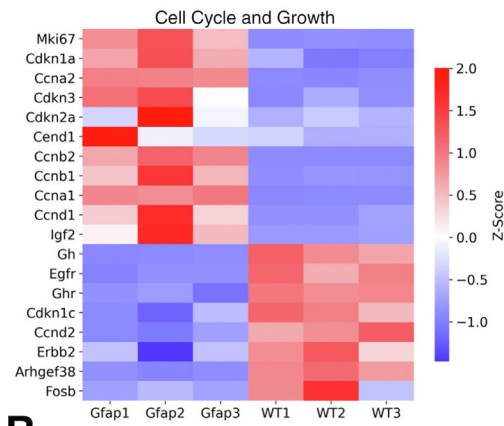
cells toward the neuronal lineage.⁴² As $GFAP^{\Delta Men1}$ pitNETs exhibited significantly elevated SHH transcript levels, we investigated whether loss of KIF3A, a ciliary motor protein required for SHH signal transduction, blocks $GFAP^{\Delta Men1}$ glia from developing a neuroendocrine phenotype. To further stimulate gastric neuroendocrine hyperplasia, $GFAP^{\Delta Men1}$ mice were crossed onto a somatostatin null (*Sst*^{-/-}) background. Somatostatin (SST) suppresses hormone secretion and gene expression, including gastrin, thus removal of *Sst*-mediated feedback inhibition increases gastrin levels.¹⁴ The effect of *Kif3a* deletion on neuroendocrine hyperplasia was accomplished by breeding $GFAP^{\Delta Men1}; Sst^{-/-}$ mice onto a *Kif3a*^{FL/FL} genetic background ($GFAP^{\Delta Men1}; \Delta Kif3a$). We next investigated whether *Kif3a* deletion could reverse the gastric hyperplasia observed in $GFAP^{\Delta Men1}$ mice. Compared with littermate controls, $GFAP^{\Delta Men1}; \Delta Kif3a$ mice more frequently presented with severe dermatitis and polycystic livers, and thus were euthanized and necropsied at 12 months of age. $GFAP^{\Delta Men1}; \Delta Kif3a$ mice exhibited reduced hyperplasia in the corpus and gastric antrum compared with age-matched $GFAP^{\Delta Men1}$ mice (Figure 8, A). To determine the effect of *Kif3a* deletion on enteroendocrine cell composition, we analyzed the expression of CHGA and gastrin in the stomach after sequential deletion of *Sst*, *Men1*, and *Kif3a* genes. Whereas $GFAP^{\Delta Men1}$ mice exhibited hyperplasia of CHGA⁺ and gastrin⁺ cells, additive deletion of KIF3A appeared to reverse these events (Figure 8, A). These observations were supported by associated fluctuations in *Chga* and *Gast* transcript levels. Whereas deleting *Men1* significantly increased the expression of *Chga* and *Gast* mRNA in the gastric antra, loss of *Kif3a* in the presence of *Sst* and *Men1* deletions inhibited this induction (Figure 8, B–C). Similarly, analysis of gastric antral extracts from these mice showed reduced gastrin peptide levels in $GFAP^{\Delta Men1}; \Delta Kif3a$ mice compared with those carrying the *Men1* deletion alone (Figure 8, D). Thus, blockade of SHH-mediated signaling in enteric $GFAP^+$ cells attenuated neuroendocrine cell hyperplasia in the stomach.

SHH Signaling Through Primary Cilia Modulates GFAP Expression

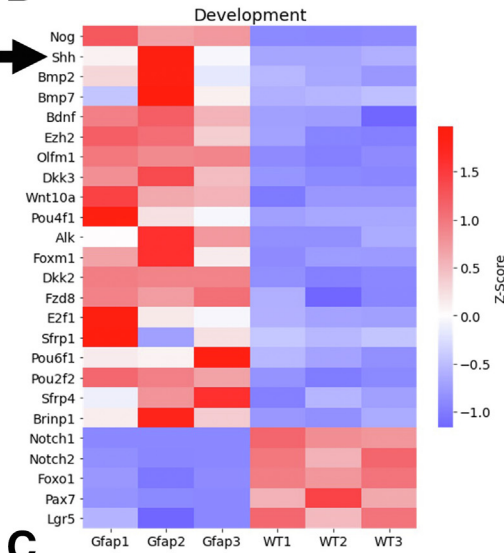
Because disruption of SHH signaling on $GFAP^+$ /menin-deficient cells resulted in reduced neuroendocrine cell hyperplasia, we further investigated a potential mechanism to bridge these events. We first confirmed that deletion of *Kif3a* resulted in the impairment of primary cilia on $GFAP^+$

Figure 6. (See previous page). Transcriptome-wide analysis of gastric neuroendocrine hyperplasia and NENs identifies a role for glial-to-neural reprogramming in epithelial differentiation. (A) Volcano plot of significant DEGs in gastric antra of wild type and $GFAP^{\Delta Men1}$ mice. (B) Volcano plot of significant DEGs in pooled WT pituitaries and pitNETs of $GFAP^{\Delta Men1}$ mice. Heat maps of significant DEGs mapped to neuroendocrine differentiation in $GFAP^{\Delta Men1}$ gastric antra (C) and pitNETs (D). Heatmap of significant DEGs mapped to the neuroglial lineage in $GFAP^{\Delta Men1}$ gastric antra (E) and pitNETs (F) compared with littermate WT controls. Arrow indicates GFAP as among the genes most significantly downregulated in tumors. (G) Immunofluorescent staining for GRP and SYP in WT and $GFAP^{\Delta Men1}$ gastric antra, shown as green and red respectively. Insets: Colocalization of GRP and SYP in the gastric mucosa (yellow). (H) Immunofluorescent staining for GRP and the nerve fiber marker NF-H, indicating localization of NF-H to the myenteric plexus, with no overlap among GRP⁺ cells of the mucosa. (I) Staining of a WT mouse gastric antrum with non-adsorbed and pre-adsorbed GRP antibody to confirm antibody specificity. (J) Quantitation of *Syp* and *Grp* mRNA following 48-hour siRNA-mediated silencing of *Men1* in rat EGCs. N = 3 independent experiments; **P* < .05 and ***P* < .01 by unpaired Student *t* test. Data are represented as mean ± standard deviation.

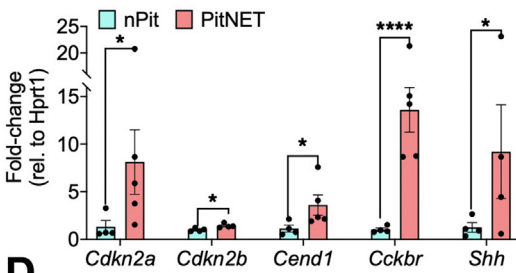
A *GFAP Δ Men1* PitNET vs WT Pituitary



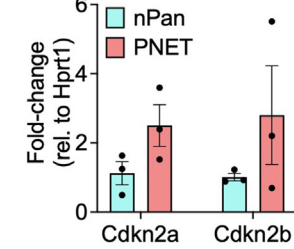
B



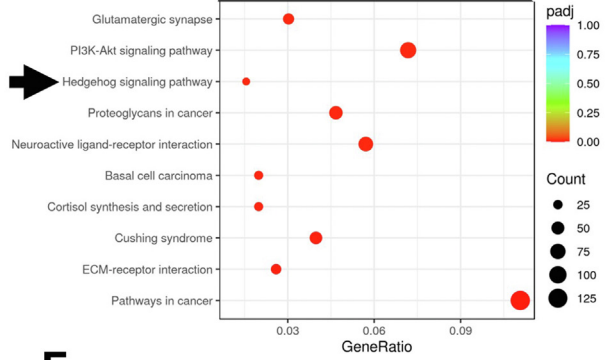
C



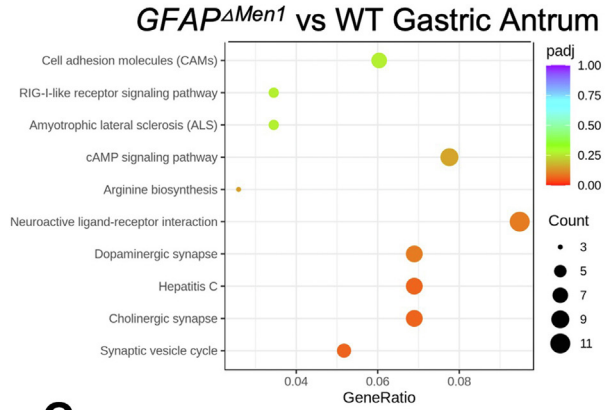
D



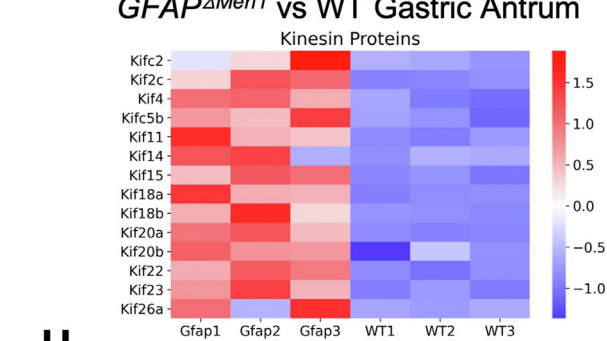
E *GFAP Δ Men1* PitNET vs WT Pituitary



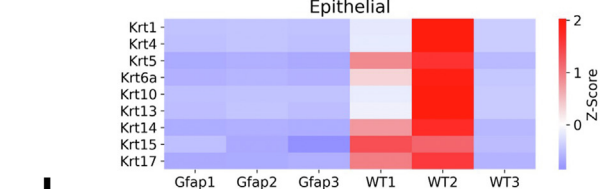
F



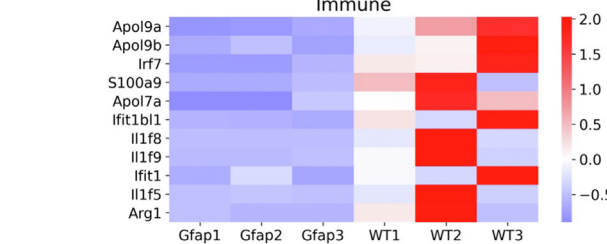
G



H



I



cells. Shortened primary cilia were shown by immunostaining for acetylated tubulin-positive hair-like projections on GFAP⁺ cells of the gastric antrum. Compared with WT mice, *GFAP^{ΔMen1;ΔKif3a}* mice exhibited significantly shortened primary cilia on GFAP⁺ cells residing in the gastric mucosa (Figure 9, A–B). Hedgehog signaling is mediated through activation of the GLI1/2/3 family of transcriptional effectors.⁴³ Thus, we assessed whether deleting *Kif3a* affects the expression of GLI2, a known suppressor of gastrin gene expression in antral G cells.⁴⁴ Whereas GFAP-directed *Men1* deletion increased antral GLI2 expression, loss of *Kif3a* reduced the expression of GLI2 protein without significantly influencing transcript levels (Figure 9, C–D). We next assessed whether *GFAP^{ΔMen1;ΔKif3a}* mice showed reduced GFAP-tdTomato fluorescence compared with *GFAP^{ΔMen1}* mice with intact primary cilia. As expected, loss of GFAP-tdTomato fluorescence was reversed in the *GFAP^{ΔMen1;ΔKif3a}* mice (Figure 9, E–F). Further, *Kif3a* deletion was associated with a trending but nonsignificant increase in antral *Gfap* mRNA expression (Figure 9, G), suggesting that modulation of GFAP by hedgehog signaling is most apparent at the protein level.

SOX10-driven Deletion of Men1 Recapitulates Hyperplastic Reprogramming of the Gastric Epithelium and Leads to Accelerated Development of PNETs

GFAP is expressed at low levels in nestin⁺ neural stem cells and turns on more strongly in terminally differentiated cells along the glial lineage in addition to other cell types, including stellate cells.⁴⁵ Therefore, we postulated that targeting *Men1* deletion by a more specific driver of glial cell specification might potentiate NET development. The nuclear transcription factor *Sry*-related HMG Box gene 10 (*Sox10*) is expressed by neural crest cells and its expression is maintained in glial and melanocyte cell lineages, but not in other neural crest cell derivatives.⁴⁶ Thus, we conditionally deleted *Men1* in *Sox10*-expressing cells using the *Sox10 Cre* system expressed on the same *Sst^{-/-}* background described previously. Unlike *GFAP^{ΔMen1}* mice that showed no apparent adverse health effects, *Sox10^{ΔMen1}* mice initially presented with reduced body weight and increased morbidity by 10 weeks of age; however, no significant fluctuations in gastric pH were observed (Figure 10, A–C). These events were later circumvented by delaying the age of weaning by 1 week and providing mice with moistened chow. Following these interventions, *Sox10^{ΔMen1}* mice

showed similar survival to littermate controls with no signs of adverse health or weight loss.

We next assessed whether surviving *Sox10^{ΔMen1}* mice aged 10 to 12 months developed endocrine hyperplasia akin to *GFAP^{ΔMen1}* mice. Four of 7 *Sox10^{ΔMen1}* mice (57%) presented with PNETs, with the incidence being slightly higher in females compared with male mice when age-matched (60% vs 50%) (Table 2; Figure 10, D). Like *GFAP^{ΔMen1}* mice, *Sox10^{ΔMen1}* mice also exhibited significantly elevated serum GCG levels compared with *Sst^{-/-}* littermate controls (Figure 10, E). Intriguingly, serum INS1 levels were too low for detection using the same high range standard curve for INS1 determination in *GFAP^{ΔMen1}* sera (1 ng/mL as the limit of detection). Surprisingly, glucose levels also trended lower in *Sox10^{ΔMen1}* mice (Figure 10, F). Although no pituitary tumors were observed in this strain at 10 to 12 months of age, *Sox10^{ΔMen1}* mice exhibited a trending but nonsignificant increase in circulating prolactin levels (Figure 10, G). Subsequent histological analysis of PNETs revealed rosette-like features typical of well-differentiated NETs (Figure 10, H). PNETs exhibited strong immunoreactivity for SYP; however, CHGA expression was restricted to a discreet cell population. Robust SYP expression overlapped with GCG, whereas CHGA⁺ cells appeared to overlap with INS1-expressing cells within tumors (Figure 9, E). Moreover, SYP⁺ tumor cells did not overlap with NF-H⁺ nerve fibers, indicating that tumor cells neither arise from, nor associate with nerve fibers (Figure 9, E).

An additional 21-month-old male mouse heterozygous for *Men1* deletion (*Men1^{FL/+}*) presented with PNETs, severe corpus hyperplasia, and multiple macroscopic antral tumors (Table 2; Figure 9, F). Subsequent staining for endocrine markers identified the presence of a CHGA⁺/SYP⁺ gastric NET in the fundic submucosa (Figure 9, G). Moreover, the gastric antrum was characterized by hyperplasia of CHGA⁺, SYP⁺, and gastrin⁺ cells, consistent with increased serum gastrin levels in these mice (Figure 9, G–H). Similar to *GFAP^{ΔMen1}* mice, all G cells expressed SYP but not CHGA. Thus, cell autonomous inactivation of *Men1* using *Sox10 Cre* as a more selective driver of the glial lineage accelerated the development of PNETs and recapitulated the hyperplastic gastric phenotype observed in *GFAP^{ΔMen1}* mice.

Discussion

Progress in understanding GEP-NET pathogenesis is impeded by a lack of comprehensive in vivo models, in part due to tissue heterogeneity from which the neoplasms arise, and the paucity of driver mutations identified that precede

Figure 7. (See previous page). Transcriptome analysis identifies potential pathways in neuroendocrine differentiation leading to gastric neuroendocrine hyperplasia and NET development in *GFAP^{ΔMen1}* mice. Heat maps of significant DEGs mapped to cell cycle regulation (A) and development (B) in *GFAP^{ΔMen1}* pitNETs compared with WT pituitaries. (C) Validation of select DEGs in pitNETs vs WT pituitary by qPCR. N = 4–5 mice per group. WT pituitary group represents 4 samples of 3 pooled pituitaries, for a total of 12 tissues in this group. **P* < .05; ****P* < .001 by 2-way analysis of variance. (D) Cross-validation of select pitNET-enriched transcripts in *GFAP^{ΔMen1}* PNETs and WT pancreas. Data are represented as mean ± standard deviation. (E) Kyoto Encyclopedia of Genes and Genomes (KEGG) Ontology Pathway analysis of wild type pituitary and *GFAP^{ΔMen1}* pitNETs showing the number of genes mapped to enriched pathways and their level of statistical significance. (F) KEGG Ontology Pathway analysis of gastric antra from WT and *GFAP^{ΔMen1}* mice showing the number of genes mapped to enriched pathways and their level of statistical significance. (G) Heat map showing enrichment of kinesin motor protein transcripts in *GFAP^{ΔMen1}* pitNETs. Heat maps depicting downregulation of cytokeratins (H) and immune-related transcripts (I) in *GFAP^{ΔMen1}* antral extracts.

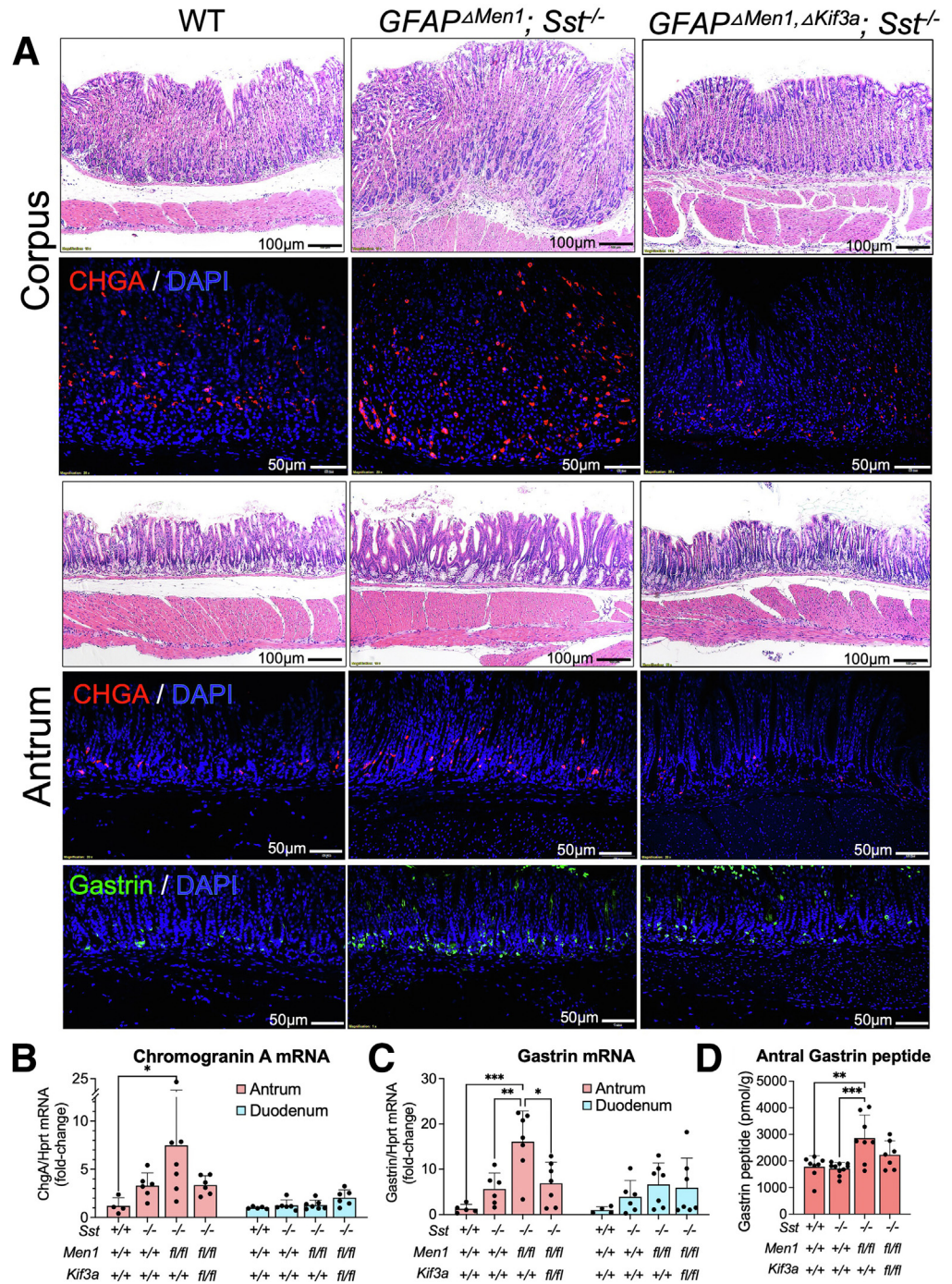


Figure 8. Blockade of SHH signaling in GFAP⁺ cells attenuates gastric neuroendocrine differentiation in *GFAP^{ΔMen1}* mice. (A) Representative hematoxylin and eosin (H&E) and immunofluorescent images of corpus and gastric antrum of *GFAP^{ΔMen1}; Sst^{-/-}*, *GFAP^{ΔMen1}; ΔKif3a; Sst^{-/-}* and littermate control mice showing reduced numbers of CHGA- and gastrin-positive cells with additive *Kif3a* deletion. CHGA (B) and gastrin (C) mRNA expression is reduced in the gastric antra following *Kif3a* deletion. (D) Expression of antral gastrin peptide among the different genotypes as evaluated by enzyme immunoassay. N = 7–8 mice per group; ***P* < .01; ****P* < .001. All data are represented as mean ± standard deviation.

malignancy.⁴⁷ We report here that conditional deletion of the tumor suppressor protein *Men1* (menin) in GFAP⁺ cells induced neuroendocrine cell hyperplasia in the gastric antrum and the development of neuroendocrine tumors in the pituitary and pancreas.

Neuroendocrine cell hyperplasia and NET development coincided with an unexpected loss of GFAP expression and induction of neuronal and neuroendocrine-related genes in the stomach, pancreas, and pituitary. In contrast to pituitary

and pancreatic NETs, which exhibited global reduction in GFAP protein and mRNA expression, the gastric antra of *GFAP^{ΔMen1}* mice showed reduced GFAP-reporter expression but did not exhibit significant loss of GFAP at the transcript level. This observation may be explained in part by the fact that menin interacts and colocalizes with GFAP.³⁷ Hence, it remains a possibility that conditional deletion of menin in GFAP⁺ cells disrupts proper localization of GFAP, leading to altered glial cell identity and creating a microenvironment

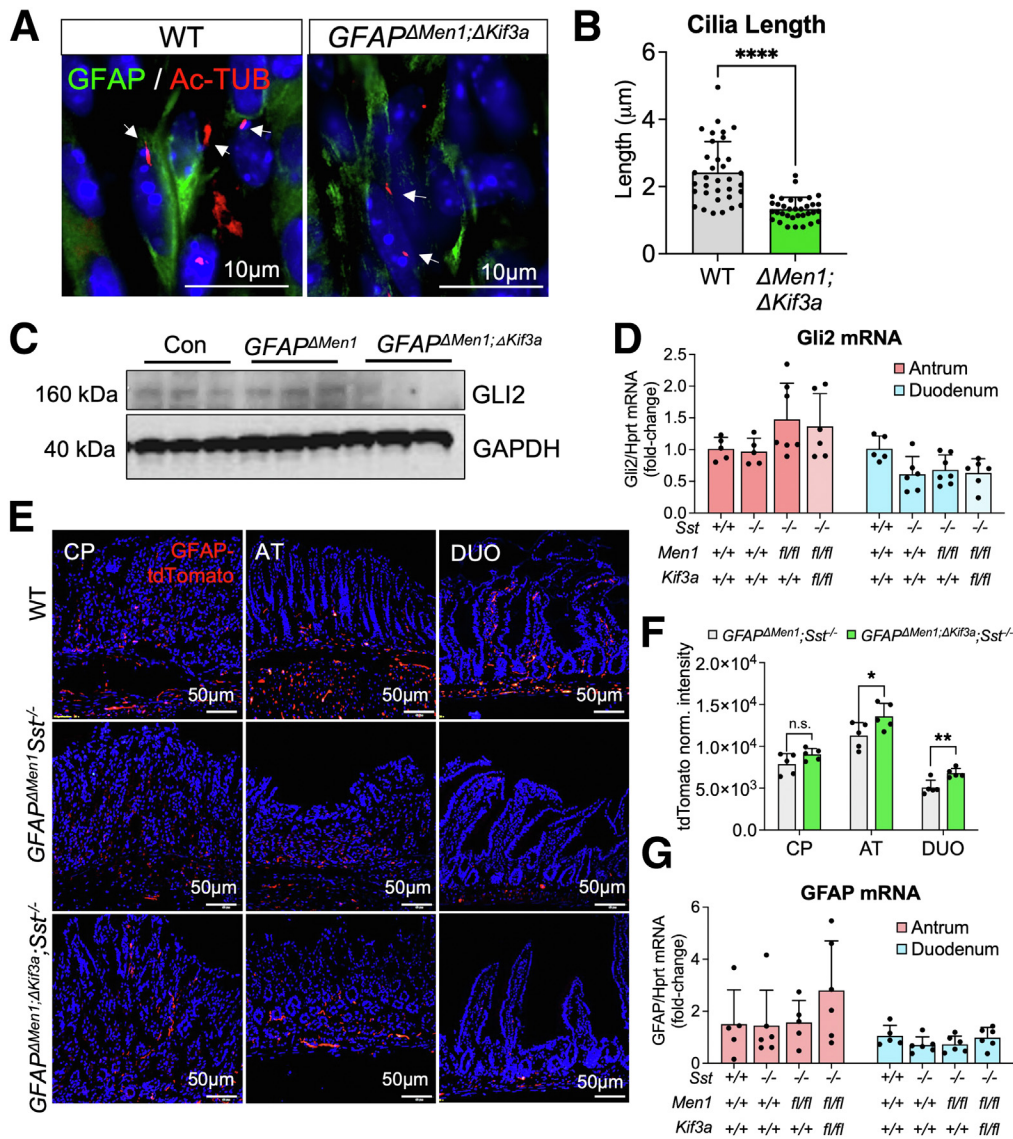


Figure 9. Loss of the ciliary motor protein KIF3A in GFAP-expressing cells impairs SHH signaling and GFAP expression. (A) Immunofluorescent staining for acetylated-tubulin (Ac-TUB) and GFAP in the gastric antra of WT and $GFAP^{\Delta Men1};\Delta Kif3a;Sst^{-/-}$ mice. Arrows indicate primary cilia marked by acetylated tubulin. (B) Quantitation of primary cilia length in GFAP-expressing cells of the gastric antrum. $N = 34$ cells counted across 10 random $1000\times$ magnification images per group. $****P < .0001$ by the unpaired Student t test. (C) Western blot of GLI2 protein in gastric antral lysates of $Sst^{-/-}$ (Con), $GFAP^{\Delta Men1};Sst^{-/-}$, and $GFAP^{\Delta Men1};\Delta Kif3a;Sst^{-/-}$ mice. $N = 3$ mice. (D) *Gli2* mRNA in gastric antra and duodenal mucosa of respective genotypes. $N = 4-7$ mice per group. (E) Representative images of cryosections of corpus (CP), gastric antrum (AT), and proximal duodenum (DUO) from WT, $GFAP^{\Delta Men1};Sst^{-/-}$ and $GFAP^{\Delta Men1};\Delta Kif3a;Sst^{-/-}$ mice expressing tdTomato. (F) Quantitation of relative tdTomato fluorescence intensity following whole tissue ex vivo imaging. $*P < .05$; $**P < .01$ by 2-way analysis of variance. (G) Quantitation of GFAP mRNA in the gastric antrum and duodenum of different groups. $N = 4-7$ mice per group. All data are represented as mean \pm standard deviation.

sufficient for tumor formation in the pancreatic islet and pituitary but not in the gastric antrum or intestine.

Similar to previous reports of conditional $Men1^{KO}$ mouse models, we did not observe the development of small intestinal gastrinomas, suggesting that additional genetic or microenvironmental factors are required to stimulate neoplastic transformation in these tissues.^{12,48-52} To identify molecular features that might inform the transition from neuroendocrine hyperplasia to NET development, we

compared the transcriptomes of hyperplastic antral tissues with well-differentiated NETs arising in this model. Although GFAP-directed $Men1$ deletion induced neural differentiation pathways at both tissue sites, NETs exhibited loss of more glial-restricted progenitor lineage-associated genes (eg, *Gfap*, *Aldh111*, *Slc1a3*, *Aqp4*, and *Olig1*) and downregulation of factors involved in directing gliogenesis (eg, *Nfia*, *Nfib*, *Zfp3611*, *Id3*, *Sox9*).⁵³⁻⁵⁷ Thus, the transition from a glial-to-neuronal cell phenotype appears to promote

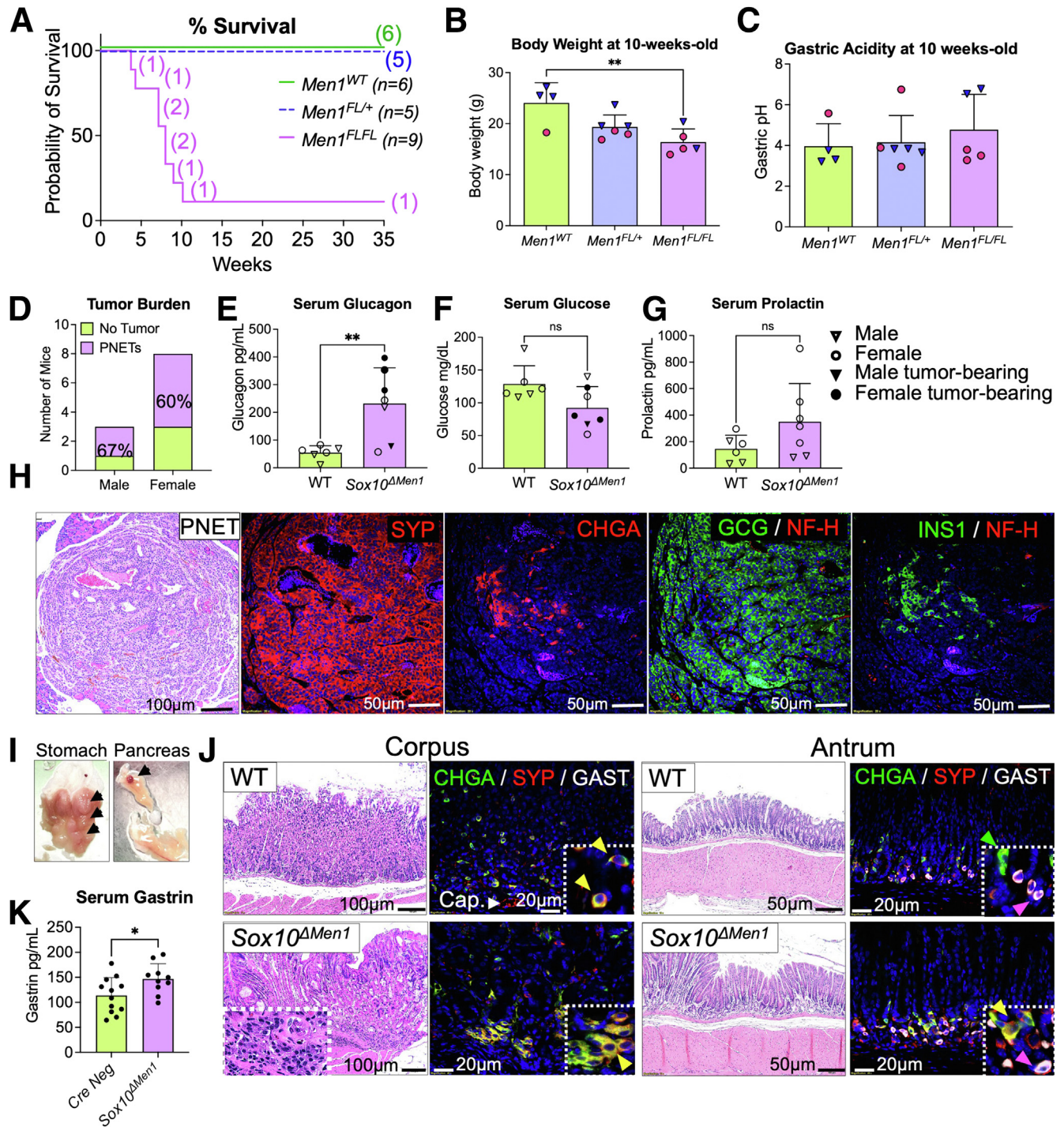


Figure 10. SOX10-driven deletion of *Men1* recapitulates hyperplastic reprogramming of the gastric epithelium and leads to accelerated development of PNETs. (A) Survival curve for $Sox10^{\Delta Men1}$ mice prior to delaying the age of weaning from 3 weeks of age to 4 weeks. Body weight (B) and gastric pH (C) of 10-week-old $Sox10^{\Delta Men1}$ mice prior to adjusting the age of weaning from 3 weeks to 4 weeks of age. Blue triangles = male mice; Red circles = female mice. (D) Number of $Sox10^{\Delta Men1}$ mice presenting with PNETs by 11 months of age, as stratified by sex. Levels of serum GCG (E) glucose (F) and prolactin (G) in $Sox10^{\Delta Men1}$ mice compared with littermate controls, with symbols indicating male and female mice with and without the tissue-involved tumors. N = 6–7 mice per group; ** $P < .01$ by the unpaired Student *t* test. (H) Representative hematoxylin and eosin and immunofluorescent images of a well-differentiated $Sox10^{\Delta Men1}$ PNET stained for neuroendocrine and hormone markers. Hormone-expressing tumor cells are negative for expression of the nerve fiber marker NF-H. (I) Macroscopic images of tissues from a 21-month-old $Sox10^{\Delta Men1}$ mouse presenting with corpus hyperplasia, multiple antral adenocarcinomas, and a PNET. (J) Hematoxylin and eosin and immunofluorescent staining of the previous stomach tissues indicating the presence of a gastric NET and neuroendocrine cell hyperplasia. Colored arrows indicate the degree of co-localization of CHGA (green), SYP (red), and gastrin (white), with several gastrin⁺ cells expressing SYP but not CHGA. (K) Serum gastrin peptide levels in 6–11-month-old $Sox10^{\Delta Men1}$ mice as evaluated by enzyme immunoassay. N = 9–12 mice per group; * $P < .01$ by the unpaired Student *t* test. All data are represented as mean \pm standard deviation.

the progression from neuroendocrine cell hyperplasia to tumor development. In support of this, NETs exhibit increased expression of genes associated with neural stem and progenitor cell status (eg, *Fabp7*, *Vim*, *Sox11*, and *Hoxb* genes) and upregulation of neural crest-secreted factors that favor neurogenesis and restrict a glial cell fate (eg, *Bmp2*, *Bmp7*, and *Shh*).^{58–64} A number of these signaling factors are components of the Hedgehog signaling pathway, known to play a role in directing neuronal differentiation at the expense of restraining gliogenesis and glial cell maturation.⁴² A role for menin in this process is highlighted by the fact that menin is a known epigenetic repressor of both canonical and non-canonical Hedgehog signaling.^{65,66} Moreover, these studies demonstrate that blockade of Hedgehog signaling-attenuated islet cell proliferation in a *Men1*-mediated insulinoma mouse model.⁶⁶ Consistent with these reports, we found that attenuation of SHH signaling by disrupting primary cilia on GFAP⁺ cells reduced neuroendocrine hyperplasia by restricting neural differentiation of GFAP⁺/menin-deficient cells toward the glial-restricted progenitor lineage.

Enteric glia exhibit a high degree of cellular plasticity within the context of their specific microenvironment.^{51,67} Indeed, they have been identified as a source of neural progenitor cells and are able to de-differentiate and trans-differentiate to other cell lineages under explicit physiological and in vitro conditions.^{15,16,68–71} However, it remains unknown whether neural crest cells or their progeny can undergo context-specific reprogramming (eg, by acquiring *MEN1* mutations) and give rise to neuroendocrine cells with hormone-secreting capabilities. Evidence to support glial or astrocytic reprogramming would challenge the long-standing paradigm that neuroendocrine tumors in the GI tract must develop from enteroendocrine cells that originate from *Lgr5*⁺ stem cells of endodermal origin.⁷² Prior work by our group using *Villin*^{Δ*Men1*} mice demonstrated that non-cell autonomous loss of menin protein in enteric GFAP⁺ glial cells induces gastrin hormone expression.^{13,14} Moreover, the loss of menin suggested crosstalk between enterocytes and enteric glia. In the current study, cell autonomous deletion of *Men1* in GFAP⁺ cells was insufficient to drive gastric NET formation. Thus, gastric NET development in *Villin*^{Δ*Men1*} mice likely requires non-glial cell autonomous signaling from the epithelium.

Furthermore, human duodenal NETs are known to express glial cell markers, with some cells within the tumor exhibiting expression of both the neuroendocrine marker SYP and the glial-specific protein S100B.^{14,73} We recently used digital spatial profiling to characterize neuroglial features in a small subset of human duodenal NETs.⁷³ Tumors exhibited reduced expression of mature neuronal and glial cell markers compared with the adjacent BGs from which 60% of these tumors are reported to originate.⁹ Collectively, these observations raise the potential for the presence of a potential hybrid transition state, in which reprogrammed enteric neural crest-derived cells escape a glial-restricted lineage and acquire a neuroendocrine phenotype.

Transcriptome-wide sequencing of the hyperplastic gastric antra of *GFAP*^{Δ*Men1*} mice identified neural lineage

genes previously reported to be upregulated in human duodenal gastrinomas emerging from the BGs, including *Hap1*, *Mn1*, and *Uchl1*.⁷³ This suggests a potential concordance between the human BGs and the pyloric antra of mice. Indeed, a recent study by Wells and colleagues reported that transplantation of human antral organoids co-cultured with human ENCCs induced the formation of highly differentiated epithelium analogous to the BGs.⁷⁴ Subsequent analysis of ENCCs identified elevated expression of the SHH-induced posteriorizing factors BMP4 and BMP7, and that inhibition of these factors in ENCCs attenuates BG formation in organoid co-cultures.⁷⁴ Consistent with our observations, ENCCs and their progeny carry the potential to direct epithelial differentiation in favor of an endocrine phenotype, and these events are strongly influenced by SHH-mediated signaling. Importantly, our observations prompt further investigation into both glial cell autonomous and non-cell autonomous mechanisms presaging these outcomes.

In summary, we report the development of 2 glial-directed mouse models of human MEN1 syndrome with the aim of defining the contribution of neural crest cell reprogramming in neuroendocrine cell differentiation and tumorigenesis. Because it remains unknown at what point during the cell's lifespan it transitions to a hormone-producing endocrine cell upon loss of menin, we used a constitutive *Cre* as reported here. Future work requires lineage tracing coincident with inducible deletion of *Men1* using glial-restricted promoters to directly track GFAP⁺ and SOX10⁺ cells in NET development. By addressing a previously uncharacterized compartment of GEP-NETs, this study carries the potential to identify a unique cell-of-origin for these neoplasms. The importance of these discoveries is underscored by the fact that GEP-NETs comprise remarkably diverse neoplasms that vary in location, mutational profile, and response to therapy. Such heterogeneity may in part be explained by divergent cellular origins for NETs as a function of different tissue sites. Previous work centered on mapping their unique transcriptional signatures suggests the potential for neuroglial reprogramming in the development of human duodenal gastrinomas. Defining the cells-of-origin and the events preceding neoplastic transformation will be critical to informing molecular signaling pathways that can then be targeted therapeutically.

Materials and Methods

Animal Studies

All animal studies received approval by the University of Arizona Institutional Animal Care and Use Committee and conform to the Animal Research: Reporting of In Vivo Experiments (ARRIVE) guidelines. Mice were housed in individually ventilated caging, with food and water ad lib. All mice were fasted overnight with water ad lib prior to blood collection. Mouse strains, Research Resource Identifiers, and vendors are listed in Table 3. *GFAP-Cre* transgenic mice on a C57BL/6J genetic background were purchased from Jackson Laboratories and bred onto a *Men1*^{FL/FL} background to conditionally delete *Men1* in GFAP-expressing cells (named *GFAP*^{Δ*Men1*}). A subset of wild type and *GFAP*^{Δ*Men1*} mice

Table 2. Summary of Phenotypes Observed in *Sox10 Cre; Men1^{FL/FL}* Mice Aged 10 to 21 Months

Men1	Pancreatic hyperplasia/tumor, n/N; average age	Pituitary adenoma, n/N	Antral hyperplasia/tumor, n/N
WT	0/6; 12.6 mo	0/6	0/6
FL/+	1/1; 21 mo • 1/1 male	0/1	1/1 (gastric carcinoid and adenocarcinoma)
FL/FL	4/7; 11 mo • 3/5 female • 1/2 male	0/7	1/7 • 1/5 female

WT, Wild-type.

were bred onto a somatostatin-null background (*Sst*^{-/-}). *GFAP*^{Δ*Men1*}; *Sst*^{-/-} mice were further bred onto a *Kif3a*^{FL/FL} background to conditionally delete *Kif3a* under the control of the *Gfap* promoter (named *GFAP*^{Δ*Men1*; Δ*Kif3a*}; *Sst*^{-/-}). WT, *GFAP*^{Δ*Men1*}, *GFAP*^{Δ*Men1*}; *Sst*^{-/-}, and *GFAP*^{Δ*Men1*; Δ*Kif3a*}; *Sst*^{-/-} mice were also bred to mice carrying a *lox-Stop-lox-tdTomato* sequence to selectively express the tdTomato fluorescent reporter in GFAP⁺ cells. *GFAP*^{Δ*Men1*} strains were necropsied at 8 to 9 months of age and between 13 and 24 months of age. All histological characterization and downstream comparisons were made using littermate controls that genotyped negative for *Cre* recombinase expression and included mice with and without the relevant floxed alleles. *Sox10-Cre* transgenic mice were bred onto the *Men1*^{FL/FL} and *Sst*^{-/-} background to generate *Sox10*^{Δ*Men1*} mice. *Sox10*^{Δ*Men1*} mice were necropsied at 10 to 12 months of age, except for one *Men1*^{FL/+} male mouse taken at 21 months old. Histological characterization and serum analyses were compared with *Cre*-negative littermate controls.

Cell and Tissue Culture

PNET organoids. Organoids were generated from four 17 to 18 month old *GFAP*^{Δ*Men1*} mice presenting with pancreatic neuroendocrine tumors. Tumors were carefully removed from adjacent pancreas tissue and washed in ice-cold Dulbecco's phosphate buffered saline (PBS) (minus Ca²⁺/Mg²⁺) containing RNase inhibitor. Tumors were minced using a razor blade, then collected in 10 mL of collagenase solution consisting of 1.5 mg/ml Type VIII collagenase, 40 μg/ml DNase I, 10 mM HEPES, and 5% fetal bovine serum (FBS) dissolved in prewarmed Dulbecco's PBS (minus Ca²⁺/Mg²⁺). Tissue was digested at 200 rpm for 40 minutes at 37 °C. The suspension was shaken 5 to 7 times prior to filtering through a 100-μm cell strainer and centrifuging at 400 × g for 5 minutes at 4 °C. The pellet was gently washed once with prewarmed media and re-pelleted. The pellet was resuspended in ice-cold Matrigel (Corning, Corning, NY), and 25 μL was pipetted into each well of a prewarmed 24-well plate. The plate was inverted and incubated at 37 °C for 15 minutes before supplementing with complete PNET organoid growth media consisting of a 1:1 solution of L-WRN conditioned media and Basal Growth Media (advanced DMEM/F12, 1× B-27 supplement, 1× N-2 supplement, 10

mM HEPES, 2 mM GlutaMAX, 1× penicillin-streptomycin, 1 mM N-acetylcysteine). Growth media was supplemented with ascorbic acid (284 μM, Sigma), INS1 (20 μg/mL, Tocris), hydrocortisone (0.25 μg/mL, Sigma), retinoic acid (100 nM, Sigma), FGF-10 (100 ng/mL, Biolegend), Y-27632 (10 μM, Tocris), and A8301 (500 nM, Tocris).

PitNET neurospheres. Primary tumor neurospheres were generated from three 17- to 18-month-old female *GFAP*^{Δ*Men1*} mice presenting with pituitary adenomas. A 4 × 2 mm piece of tissue was cut from the tumor and minced into 1-mm pieces on ice. The tissue was transferred to a 10 mL solution of Dispase/DNase solution warmed to 37 °C (0.1% dispase, 0.01% DNase, 10 mM HEPES, DPBS without calcium and magnesium) and incubated in a shaking water bath (60 rpm) at 37 °C for 80 minutes. Halfway through the incubation, the tissue was shaken manually 3 times to facilitate dissociation. The tissue was triturated 10 times with a 10 mL serological pipette, then filtered through a 40-μm cell strainer before centrifuging at 123 × g for 10 minutes at 4 °C. The cell pellet was resuspended in Neurosphere Media consisting of DMEM/F12 (ThermoFisher, Waltham, MA), 1× GlutaMAX (Invitrogen, Carlsbad, CA), 1× N2 (Gibco, Waltham, MA), 1× B-27 (Gibco), 100 U penicillin-streptomycin (Invitrogen), 10 mM HEPES (Invitrogen), 30 ng/mL mouse recombinant FGF-10 (Biolegend, San Diego, CA), and 30 ng/mL recombinant human EGF (R&D Systems, Minneapolis, MN). Cells were plated in a non-tissue culture treated 6-well plate and incubated overnight at 37 °C. Media was changed every 2 to 3 days by collecting neurospheres, centrifuging, and reseeding the pellet in fresh medium. Tumor neurosphere generation was repeated with 3 prolactinoma-bearing mice.

A rat enteric glial cell line was purchased from ATCC (#CRL-2690) and grown in DMEM supplemented with 10% FBS and 100 U penicillin-streptomycin (EGC/PK060399egfr, ATCC, Manassas, VA). Upon reaching 30% to 50% confluency, glial cells were switched to 5% FBS-containing media and used for siRNA experiments. Both the non-targeting siRNA and *Men1* siRNA consisted of a SMART-pool of 4 ON-TARGETplus siRNA constructs (#L-090784-02-0005 for *Men1* pool and #D-001810-10-05 for non-targeting pool, Dharmacon Horizon Discovery, Lafayette, CO). Cells were transfected with 25 nM siRNA using Lipofectamine 3000 without p3000 reagent according to manufacturer

instructions (ThermoFisher). Following 48 to 72 hours post-transfection, cells were harvested for downstream RNA or protein extraction.

Immunohistochemistry and Immunofluorescent Staining

Mouse tissues were fixed overnight at 4 °C in 4% paraformaldehyde. Tissues were paraffin-embedded, cut into 5- μ m sections, and placed on frosted glass slides. Slides were deparaffinized in 3 xylene washes, then rehydrated in 100%, 90%, and 70% ethanol washes. Slides were washed in TBS with 0.05% Tween-20 (TBST) before proceeding with antigen retrieval. Slides were boiled in 1 \times sodium citrate buffer pH 6.0 for 30 minutes and allowed to cool to room temperature (RT) for 20 minutes prior to washing with TBST. Slides were incubated for 1 hour at RT in blocking buffer consisting of 10% donkey serum, 1% bovine serum albumin (BSA), 0.1% Triton X-100 in TBST. In some instances, tissues were permeabilized with 0.5% Triton X-100 for 5 minutes at RT prior to blocking. Tissues were incubated in primary antibody overnight at 4 °C. Primary antibodies were prepared in blocking solution according to the dilutions listed in Table 4. Following overnight incubation, slides were washed in TBST and incubated in Alexa Fluor-conjugated secondary antibodies (Molecular Probes, Eugene, OR; Invitrogen) diluted 1:500 in 1% BSA and TBST for 1 hour at RT in the dark. Slides were washed in TBS before mounting with #1.5 coverslips using Prolong Gold anti-fade mounting medium with DAPI (Life Technologies, Rockville, MD). Immunofluorescence was visualized at 200 \times , 400 \times , and 1000 \times magnification using the Olympus BX53F epifluorescence microscope (Center Valley, PA).

For immunofluorescent staining of PNET organoids and PitNET neurospheres, organoids and neurospheres were collected and centrifuged. The pellet was resuspended in 3.7% paraformaldehyde and transferred to a 24-well 0.17-mm glass-bottom plate. Organoids and neurospheres were fixed for 20 minutes at RT, then washed with 1 \times TBST. Samples were permeabilized with 0.5% triton X-100 for 10 minutes at RT, washed, then blocked in 10% donkey serum, 1% BSA, and 0.2% triton in TBST for 1 hour at RT. Primary antibodies were diluted in 5% donkey serum 1% BSA, 0.1% triton in TBST and added to wells for overnight incubation at 4 °C. Samples were washed thoroughly with TBST and incubated for 1 hour at RT in Alexa Fluor-conjugated secondary antibodies diluted 1:500 in 1% BSA and TBST. Organoids and neurospheres were washed with TBS, then stored in TBS containing Prolong gold antifade mounting medium with DAPI. Samples were imaged at 600 \times magnification using a Nikon Ti2-E inverted microscope with a Crest X-Light V2 L-FOV Spinning Disk Confocal and a Photometrics Prime 95B-25MM Back-illuminated sCMOS Camera (Nikon, Tokyo, Japan).

Mouse tissues with endogenous tdTomato reporter expression were fixed in 4% paraformaldehyde for 1 hour on ice before dehydrating overnight at 4 °C in a solution of 30% sucrose-PBS. Tissues were then embedded in Tissue-Tek optimal cutting temperature (OCT) compound (Sakura

Finetek, Torrance, CA) and frozen on dry ice. OCT blocks were cryosectioned to a 10- μ m thickness and melted onto frosted glass slides prior to mounting with Prolong Gold anti-fade mounting medium containing DAPI. TdTomato signal was visualized at 200 \times (whole mount) and 1000 \times magnification (co-stained images) using the Olympus BX53F epifluorescence microscope. Images drawing comparisons between groups were acquired with identical laser acquisition settings (Center Valley, PA).

Antibody Pre-adsorption

Select antibodies were tested for specificity by pre-adsorption with recombinant proteins. Briefly, human recombinant protein was mixed with respective antibody at a 5-fold excess by weight. Antibody-antigen solution was diluted to a working concentration in 10% donkey serum, 1% BSA, 0.1% triton in TBST and incubated overnight at 4 °C on a rotator. The antibody-antigen solution was then used for immunohistochemistry/immunofluorescence staining as previously described and compared with staining with antibody only. Images were acquired using identical acquisition settings for comparison of fluorescence signal.

qPCR

RNA was extracted from frozen mouse tissues using the Purelink RNA Extraction Kit (Invitrogen). Tissues were homogenized with a rotor-stator homogenizer in RNA lysis buffer containing 1% β -mercaptoethanol, and RNA was isolated following manufacturer's instructions. Extracted RNA was treated with ezDNase to remove any residual genomic DNA and then prepared for cDNA synthesis using Superscript VILO IV Master Mix according to manufacturer's instructions (Invitrogen). Real-time qPCR was performed using PowerUp SYBR Green Master Mix (Invitrogen) with 20 ng cDNA added to each reaction. Predesigned forward and reverse primer sets were purchased from Integrated DNA Technologies (IDT, Coralville, IA) and used at a final 500 nM concentration. qPCR was performed using the QuantStudio 3 Real-Time PCR System (Applied Biosystems, Waltham, MA) with the following cycling conditions: 2 minutes at 50 °C, 2 minutes at 95 °C, denaturing step for 1 second at 95 °C, extension and annealing for 1 minute at 60 °C, followed by a dissociation melt curve stage to confirm primer specificity. All forward and reverse primers were purchased as validated predesigned PrimeTime qPCR Assay primer sets used for SYBR Green dye (Integrated DNA Technologies, Coralville, IA). qPCR data was expressed as fold-change using the established $2^{-\Delta\Delta C_t}$ method and log-transformed to fit a normal distribution prior to performing statistical analysis.^{75,76}

Ex Vivo Fluorescence Imaging

At 8 to 9 months of age, *GFAP Cre-tdTomato* mice were euthanized following overnight fasting, and the stomach and proximal duodenum were collected for ex vivo imaging prior to fixation for OCT embedding. The stomach and proximal duodenum were opened along the greater

Table 3. List of Mouse Strains and Vendors

Mouse strain name	Strain #	RRID #	Vendor/provider
FVB-Tg(GFAP-cre)25Mes/J	004600	IMSR_JAX:004600	Jackson Laboratories
129S(FVB)-Men1 ^{tm1.2Cre} /J	005109	IMSR_JAX:005109	Jackson Laboratories
B6.Cg-Gt(ROSA)26Sor ^{tm14(CAG-tdTomato)Hze} /J	007914	IMSR_JAX:007914	Jackson Laboratories
B6;CBA-Tg(Sox10-cre)1Wdr/J	025807	IMSR_JAX:025807	Jackson Laboratories
Sst ^{-/-}	Strain provided by Dr. Malcolm Low and described in PMID: 11413165 (not available in Jackson Laboratories to the authors' knowledge).		

RRID, Research Resource Identification.

curvature, and contents were flushed with cold PBS. Both tissues were placed in cold PBS with mucosa facing up and imaged in a dark room using a wide field fluorescence imaging system. Illumination was provided by a 300W xenon arc lamp source (LS-OF30, Sutter instruments, Novato CA). Illumination light was filtered with a 554 nm excitation filter with 23 nm bandwidth (FF01-554/23-25, Semrock Inc., Rochester NY) and delivered using a fiber bundle (LLG, Sutter Instruments). Images were collected with an 0.5" CCD Monochrome Camera (EO-1312M, Edmund Optics, Barrington NJ) with a 35 mm fixed focal length lens (#59-872, Edmund Optics) and a 594 nm long-pass filter (BLP01-594R-25, Semrock) mounted on a rigid arm above the sample plane. Images were collected with an exposure time of 60 ms and saved in 16 bit .tif format. Each day, a flat-field image was collected by imaging a white diffuse reflectance target (#58-609, Edmund Optics) to correct for spatial non-uniformity using unfiltered illumination. Additionally, a power measurement was collected for the filtered illumination light at the sample plane using a power meter (S120C, Thorlabs, Newton NJ) to adjust for day-to-day variations of light source intensity. The collected images were first normalized through division by the flat-field image and the light source power measured on the day of sample acquisition. Regions of interest were then manually drawn around the forestomach, corpus, antrum and duodenum using ImageJ. Fluorescence intensity was calculated in the region of interest and averaged over the number of valid pixels. Any pixels with 5% of saturation (eg, digital value of 65535) were discarded from the analysis.

RNA Sequencing

RNA was extracted from 3 *GFAP*^{ΔMen1} PNETs, pitNETs, and the pyloric antrum using the Purelink RNA Extraction kit as previously described (Invitrogen). Pancreas, pituitary, and antra of age-matched WT mice were used as controls. Due to its small size, 3 normal pituitaries were pooled for each sample, and a total of 3 samples were submitted for sequencing (ie, 9 WT pituitaries total). RNA was processed on the bioanalyzer for quality control prior to proceeding with mRNA library construction and bulk RNA sequencing. Due to degradation of pancreas tissues by pancreatic enzymes, only antral extracts and pituitary samples were usable for downstream library construction and sequencing. Samples were sequenced by Novogene using Illumina sequencing

platforms and the resulting calculated fragments per kilobase of transcript sequence per millions base pairs sequenced values were analyzed for differential gene expression, principal component analysis, and Gene Ontology enrichment analysis. Differential expression between WT and *GFAP*^{ΔMen1} groups was determined using the DESeq2 R package (1.20.0) using a negative binomial distribution model. *P* values were adjusted for multiple testing using the Benjamini and Hochberg's method for controlling false discovery rate and genes with adjusted *P* value < .05 were considered significantly differentially expressed. The statistical enrichment of DEGs in Kyoto Encyclopedia of Genes and Genomes pathways was tested using the clusterProfiler R package with correction for gene length bias. Gene Ontology terms with a corrected *P* value < .05 were considered significantly enriched. Heatmaps of significant DEGs assigned to specific signatures of interest were generated using Python 3 using the open-source packages Seaborn and Pandas. For each gene, the Z-score was calculated and plotted as a function of color, with the color white being fixed to a Z-score of 0.

Western Blot Analysis

Seventy-two hours following siRNA-mediated Men1 silencing, rat enteric glial cells were harvested by washing twice in cold DPBS and lysing in cold RIPA buffer containing phosphatase and protease inhibitors. Cells were collected by scraping, then homogenized by passing through a 20G needle syringe 5 times. The resulting lysate was centrifuged at 15,000 × *g* for 20 minutes at 4 °C. The supernatant was collected and used for Western blot analysis as follows. Lysates were prepared in reducing conditions in 1× SDS buffer with 5% β-mercaptoethanol and denatured by boiling at 95 °C for 5 minutes. Fifteen μg of protein was loaded into a NuPage 4% to 12% Bis-Tris Mini Protein Gel and allowed to migrate for 1 hour at 140 V in 1× MOPS Gel Electrophoresis Buffer. Proteins were transferred onto a pre-wetted polyvinylidene fluoride membrane using the iBlot2 transfer system (P0 setting, 7 minutes), then blocked in 5% BSA TBST for 1 hour at RT. Membranes were incubated overnight at 4 °C in primary antibody diluted in blocking buffer at the dilutions listed in Table 4. Membranes were washed in TBST, then incubated for 1 hour at RT in a corresponding host IgG horseradish peroxidase (HRP)-conjugated secondary antibody diluted 1:3000 in blocking buffer. Membranes were washed again in TBST and incubated in

Table 4. List of Primary Antibodies and Dilutions

Primary antibodies	Vendor	Catalog #	RRID #	Dilution/application
Menin (Rabbit pAb)	Bethyl Laboratories	A300-105A	AB_2143306	1:2,000 (IHC/IF TSA) 1:10,000 (WB)
Chromogranin A	Abcam	15160	AB_301704	1:100 (IHC/IF)
Synaptophysin	Cell Signaling Technologies	9020	AB_2631095	1:200 (IHC/IF)
Irx-2	Abcam	196755		1:100 (IHC/IF)
Ki-67	Cell Signaling Technologies	9449	AB_2797703	1:400 (IHC/IF)
α -smooth muscle actin	Abcam	5694	AB_222302	1:200 (IHC/IF)
Glucagon	Cell Signaling Technologies	2760	AB_659831	1:100 (IHC/IF)
Insulin	Cell Signaling Technologies	3014	AB_2126503	1:1000 (IHC/IF)
GFAP (Rabbit pAb)	Dako Agilent Technologies	Z0334	AB_10013382	1:400 (IHC/IF) 1:2000 (WB)
GFAP (Rat mAb)	Invitrogen	13-0300	AB_2532994	4 μ g/mg lysate (IP)
GFAP (Chicken pAb)	Invitrogen	PA1-10004	AB_1074620	1:1000 (IHC/IF)
Neurofilament-H	Novus Biologicals	NBP1-05209	AB_1556328	1:100 (IHC/IF)
S100B	Abcam	ab52642	AB_882426	1:200 (IHC/IF)
p75 ^{NTR}	Abcam	ab52987	AB_881682	1:1000 (IHC/IF)
ACTH	Novus Biologicals	NBP2-32911	AB_1069955	1:100 (IHC/IF)
Growth hormone	R&D Systems	AF1067	AB_354573	1:100 (IHC/IF)
Nestin	Novus Biologicals	NB100-1604	AB_2282642	1:500 (IHC/IF) 1:100 (ICC/IF)
Sox2	Novus Biologicals	NB110-37235	AB_792070	1:200 (ICC/IF)
Pit-1	Novus Biologicals	NBP1-92273	AB_11030310	1:500 (IHC/IF)
Prolactin	Abcam	183967	AB_2814839	1:200 (IHC/ICC/IF)
Gastrin (Rabbit mAb)	Dako Agilent Technologies	A0568	AB_2757270	1:1000 (IHC/IF)
Gastrin (Goat pAb)	Santa Cruz Technologies	Sc-7783	AB_2108261	1:1000 (IHC/IF)
Acetylated-tubulin	Sigma	MABT868	AB_2819178	1:200 (IHC/IF)
Gastrin-releasing peptide	Invitrogen	PA5-115272	AB_2899908	1:200 (IHC/IF)
GAPDH	Cell Signaling Technologies	5174S	AB_10622025	1:2000 (WB)
Gli2	Santa Cruz Technologies	271786	AB_10708124	1:1000 (WB)

ICC, immunocytochemistry; IF, immunofluorescence; IHC, immunohistochemistry; IP, immunoprecipitation; RRID, Research Resource Identification; TSA, tyramide signal amplification; WB, Western blot.

Pierce ECL reagent (ThermoFisher) for 1 minute prior to developing on film in a dark room.

For analysis of tissue extracts, gastric antra of 8- to 9-month-old mice were homogenized in ice-cold RIPA buffer using a rotor-stator homogenizer. Samples were centrifuged at $15,000 \times g$ for 15 minutes, and the supernatant (20 μg) was evaluated for Gli2 protein expression (Table 5).

Immunoprecipitation Assay

Immunoprecipitation of menin was performed in rat enteric glial cells. Prior to lysis, cells were collected in ice-cold DPBS, centrifuged, and washed once with cold DPBS. The cell pellet was resuspended in cytoplasmic lysis buffer to generate a cytoplasmic extract. Buffer was supplemented with $1 \times$ HALT protease and phosphatase inhibitor. Cytoplasmic extracts were pipetted up and down $20 \times$, incubated on ice for 10 minutes, then vortexed for 15 seconds prior to centrifuging at $15,000 \times g$ for 5 minutes at 4°C . The supernatant was saved as the cytoplasmic fraction. Protein concentration in freshly prepared lysates was evaluated by bicinchoninic assay. To form an antigen-antibody complex, 1 mg lysate was

incubated with either mouse anti-menin monoclonal antibody (Bethyl Laboratories, #A500-003A, $3\mu\text{g}$ per mg lysate) or mouse IgG1 Isotype control (Cell Signaling Technologies, $3\mu\text{g}$ per mg lysate) overnight at 4°C . Fifty μL of prewashed Protein A/G agarose beads (Pierce, #20423) was added to each antigen-antibody complex and incubated for 2 hours at 4°C on a rotator. Bead-complexes were pelleted at $3000 \times g$ for 2 minutes and washed 6 times with lysis buffer. Bound proteins were eluted by mixing with $2 \times$ SDS sample buffer. Samples were incubated at 50°C for 10 minutes, vortexed briefly, then centrifuged to remove beads. Dithiothreitol was added to the protein suspension at a final concentration of 10 mM prior to boiling at 95°C for 5 minutes. Samples were then evaluated by Western blot as previously described. Extracts were probed using rabbit anti-GFAP antibody (Dako Agilent Technologies, #Z033429, 1:3000). Immunoprecipitation was repeated 3 times in independent experiments and quantified via densitometry analysis using Image J Fiji software.

Hormone Immunoassays

GCG hormone was evaluated in mouse serum using the Mouse Glucagon enzyme-linked immunosorbent assay

Table 5. List of RT-qPCR Primers From Integrated DNA Technologies

Gene	Primer sequence 1 (5' to 3')	Primer sequence 2 (5' to 3')	IDT PrimeTime ID
<i>Chga</i>	CCAAGGTGATGATGAAGTGCCT	TGGTGTGCGCAGGATAGAGA	Mm.PT.58.41352258
<i>Syp</i>	CAGACAGGAAACACATGCAAG	TCTCCTTGAACACGAACCATAG	Mm.PT.58.29275406
<i>Gfap</i>	GCATCTCCACAGTCTTTACCA	AACCGCATCACCATTCCCTG	Mm.PT.58.31297710
<i>Gfap</i>	CATCTCCACCGTCTTTACCAC	AACCGCATCACCATTCCCTG	Rn.PT.58.36145160
<i>S100b</i>	TCACTTTGTCCACCACTTCC	GCCCTCATTGATGTCTTCCAT	Rn.PT.58.36785742
<i>Men1</i>	CCCAAGCATGATCTTCAGACA	CCCACATCCAGTCCCTCTT	Mm.PT.58.30625021
<i>Men1</i>	CATCTCTGAGACCTAGAGCCT	CACATCCAGTCTCTCTTCAGC	Rn.PT.58.9524749
<i>Chgb</i>	CCTTTCTCTTCACCTTTGACCT	CCTATCCAAGTCCAGTGTTC	Mm.PT.58.11605373
<i>Eno2</i>	ACATCCATACCGATCACCATC	CAAGGACAAGTATGGCAAGGA	Mm.PT.58.31414881
<i>Prl</i>	ATATCAGCAACAGGAGGAGTG	GTTCTCTCAGGCCATCTTGG	Mm.PT.58.9092137
<i>Vip</i>	GAGTATCAGGAATGCCAGGAA	GAACCTCAGCACCCCTAGACAG	Mm.PT.58.32346790
<i>Gast</i>	CCAAAGTCCATCCATCCGTAG	TCCTCAACACTTCATAGCAGAC	Mm.PT.58.9850738
<i>Grp</i>	CCTTGTCGTTGTCCCTTCAG	CCTCTCAGTCTCCAGCCT	Mm.PT.58.41177438
<i>Grp</i>	CCTTGTCATGGTCCCTTCAG	ATGGCAGCTACTTCAGTGATG	Rn.PT.58.45266321
<i>Gli2</i>	ATCATGCGTTGTAGGTCGAG	CATCTCCATGACTACCTCAACC	Mm.PT.58.11001473
<i>Cdkn2a</i>	CTCTGCTCTTGGGATTGGC	GTGCGATATTTGCGTTCCG	Mm.PT.58.43961185
<i>Cdkn2b</i>	GTGCACAGGTCTGGTAAGG	AGATCCCAACGCCCTGAA	Mm.PT.58.7138437
<i>Cend1</i>	CTCACCTCTGGGCATTATATGG	GAAACTCCTGAGCACTCCTC	Mm.PT.58.8515727
<i>Cckbr</i>	CAGAAAGATCACCGCATAAAGG	TCCCTCCTCAACAGCAGTAG	Mm.PT.58.45922724
<i>Shh</i>	CGTAAGTCCTTACCAGCTTG	GAATCCAAAGCTCACATCCAC	Mm.PT.58.14105875
<i>Atp4b</i>	CCTCTTTCCCATACACGTC	ATCTATGTGCTGATGCAGACC	Mm.PT.58.5892771
<i>Gif</i>	CTTGGTAGGTTGCTCAGGTG	AGGCTATTGTGGAGAAGATCAG	Mm.PT.58.13185585
<i>Lgr5</i>	GTCAAAGCATTTCAGCAAGA	CTCCAACCTCAGCGTCTTC	Mm.PT.58.12492947
<i>Muc5ac</i>	CTGGTTGAGTGGTTGTGTGT	CCCATGTGTATTCTCTCCCA	Mm.PT.58.42279692
<i>Muc6</i>	GCAGTTGGAGACACAAAGGTA	CATGACATCCACTCTCACACC	Mm.PT.58.33323120
<i>Hprt1</i>	AACAAAGTCTGGCCTGTATCC	CCCCAAAATGGTTAAGGTTGC	Mm.PT.39a.22214828
<i>Hprt1</i>	GCTTTTCCACTTTCGCTGATG	GGTGAAAAGGACCTCTCGAAG	Rn.PT.39a.22214832

RT-qPCR, Real-time quantitative polymerase chain reaction.

(ELISA) Kit according to manufacturer's instructions (Crystal Chem, #81518). Serum was diluted 1:10 (10 μ L serum per well) and incubated with anti-mouse GCG and HRP-secondary antibody overnight at 4 °C. Glucagon concentration was determined by HRP enzymatic activity, and the absorbance at 450 nm was averaged across duplicate wells. INS1 hormone was measured in mouse serum using the Ultra Sensitive Mouse Insulin ELISA Kit (Crystal Chem, #90080). Five μ L serum (1:20) was evaluated in duplicate and incubated with anti-mouse INS1 antibody overnight at 4 °C. INS1 concentration was interpolated from a high range standard curve of 1–64 ng/mL). Serum glucose was measured using a Mouse Glucose Assay Kit (Crystal Chem, #81692). Two μ L serum (1:50) was incubated with an oxidizing enzyme solution for 10 minutes at 37 °C to yield hydrogen peroxide and generate a red dye. Absorbance at 505 nm was measured and averaged across technical duplicates. Glucose concentration was interpolated from a standard curve ranging from 10.5 to 675 mg/dL. Serum prolactin levels were measured using the Mouse Serum Prolactin ELISA Kit (Invitrogen, #EMPRL). Serum was diluted 1:20 (5 μ L serum per well) and incubated with anti-mouse prolactin antibody overnight at 4 °C. HRP-secondary enzymatic activity was evaluated by measuring absorbance at 450 nm, and optical density values were averaged prior to interpolating concentrations from a standard curve of 27.43 to 20,000 pg/mL.

Gastrin peptide was evaluated in mouse serum using the Gastrin Enzyme Immunoassay according to manufacturer's instructions (Sigma, #RAB0200). Serum was diluted 1:4 (25 μ L serum per well) and incubated with biotinylated gastrin peptide anti-gastrin-1 antibody overnight at 4 °C. Gastrin concentration was determined by HRP enzymatic activity, and the average absorbance at 450 nm was calculated across duplicate wells. Gastrin concentration was interpolated from a standard curve of 0.1 to 1000 pg/mL gastrin-1 peptide that was plotted using a 4-parameter logistic regression. For tissue, gastrin peptide was extracted from the antra of 8- to 9-month-old mice by boiling tissues in 200 μ L of nuclease-free water and vigorously vortexing. The resulting solution was centrifuged to pellet debris, and 50 μ L of the supernatant was evaluated in duplicate.

Gastric Acid Determination

Following overnight fasting and necropsy, whole stomachs were removed, opened, and flushed with 5 mL of 0.9% saline solution. The stomach acid-solution was centrifuged at 2000 $\times g$ for 5 minutes, and the supernatant was collected for pH determination using a pH meter (Orion Star A111). The hydrogen ion concentration was measured by base titration with 0.005 N sodium hydroxide. Acid levels were calculated following normalization to mouse body weight.

Statistical Analysis

Assays comparing one parameter (eg, gastrin hormone) across 2 genotypes were evaluated for statistical significance by applying the unpaired Student *t* test. All qPCR data

expressed as fold-change ($2^{-\Delta\Delta Ct}$) were log-transformed to fit a normal distribution prior to performing statistical analysis. Comparisons consisting of 3 or more genotypes or groups were evaluated for significance using 1-way analysis of variance, with Tukey post-test. Group comparisons of 2 or more parameters (eg, multiple genes) across genotypes and tissues were evaluated for significance using 2-way analysis of variance with Sidak post-test. Significance was determined as **P* < .05, ***P* < .01, ****P* < .001, *****P* < .0001 using Graphpad Prism (v9) software.

References

1. Dasari A, Shen C, Halperin D, Zhao B, Zhou S, Xu Y, Shih T, Yao JC. Trends in the incidence, prevalence, and survival outcomes in patients with neuroendocrine tumors in the United States. *JAMA Oncol* 2017; 3:1335–1342.
2. Lee MR, Harris C, Baeg KJ, Aronson A, Wisnivesky JP, Kim MK. Incidence trends of gastroenteropancreatic neuroendocrine tumors in the United States. *Clin Gastroenterol Hepatol* 2019;17:2212–2217.e1.
3. Schimmack S, Svejda B, Lawrence B, Kidd M, Modlin IM. The diversity and commonalities of gastroenteropancreatic neuroendocrine tumors. *Langenbecks Arch Surg* 2011;396:273–298.
4. Thakker RV. Multiple endocrine neoplasia type 1 (MEN1). *Best Pract Res Clin Endocrinol Metab* 2010;24:355–370.
5. Thakker RV, Newey PJ, Walls GV, Bilezikian J, Dralle H, Ebeling PR, Melmed S, Sakurai A, Tonelli F, Brandi ML; Endocrine Society. Clinical practice guidelines for multiple endocrine neoplasia type 1 (MEN1). *J Clin Endocrinol Metab* 2012;97:2990–3011.
6. Waldum HL, Sandvik AK, Syversen U, Brenna E. The enterochromaffin-like (ECL) cell. Physiological and pathophysiological role. *Acta Oncol* 1993;32:141–147.
7. Chao C, Hellmich MR. Gastrin, inflammation, and carcinogenesis. *Curr Opin Endocrinol Diabetes Obes* 2010; 17:33–39.
8. Jain RN, Samuelson LC. Differentiation of the gastric mucosa. II. Role of gastrin in gastric epithelial cell proliferation and maturation. *Am J Physiol Gastrointest Liver Physiol* 2006;291:G762–G765.
9. Duan S, Rico K, Merchant JL. Gastrin: from physiology to gastrointestinal malignancies. *Function (Oxf)* 2021; 3:zqab062.
10. Anlauf M, Perren A, Meyer CL, Schmid S, Saremaslani P, Kruse ML, Weihe E, Komminoth P, Heitz PU, Klöppel G. Precursor lesions in patients with multiple endocrine neoplasia type 1-associated duodenal gastrinomas. *Gastroenterology* 2005;128:1187–1198.
11. Vanoli A, La Rosa S, Klersy C, Grillo F, Albarello L, Inzani F, Maragliano R, Manca R, Luinetti O, Milione M, Doglioni C, Rindi G, Capella C, Solcia E. Four neuroendocrine tumor types and neuroendocrine carcinoma of the duodenum: analysis of 203 cases. *Neuroendocrinology* 2017;104:112–125.
12. Crabtree JS, Scacheri PC, Ward JM, Garrett-Beal L, Emmert-Buck MR, Edgemon KA, Lorang D, Libutti SK, Chandrasekharappa SC, Marx SJ, Spiegel AM,

- Collins FS. A mouse model of multiple endocrine neoplasia, type 1, develops multiple endocrine tumors. *Proc Natl Acad Sci U S A* 2001;98:1118–1123.
13. Sundaresan S, Kang AJ, Hayes MM, Choi EK, Merchant JL. Deletion of Men1 and somatostatin induces hypergastrinemia and gastric carcinoids [published correction appears in *Gut* 2017;66:2012]. *Gut* 2017;66:1012–1021.
 14. Sundaresan S, Meiningner CA, Kang AJ, Photenhauer AL, Hayes MM, Sahoo N, Grembecka J, Cierpicki T, Ding L, Giordano TJ, Else T, Madrigal DJ, Low MJ, Campbell F, Baker AM, Xu H, Wright NA, Merchant JL. Gastrin induces nuclear export and proteasome degradation of menin in enteric glial cells. *Gastroenterology* 2017;153:1555–1567.e15.
 15. Furlan A, Dyachuk V, Kastri ME, Calvo-Enrique L, Abdo H, Hadjab S, Chontorotzea T, Akkuratova N, Usoskin D, Kamenev D, Petersen J, Sunadome K, Memic F, Marklund U, Fried K, Topilko P, Lallemand F, Kharchenko PV, Ernfors P, Adameyko I. Multipotent peripheral glial cells generate neuroendocrine cells of the adrenal medulla. *Science* 2017;357:eaal3753.
 16. Fielitz K, Althoff K, De Preter K, Nonnekens J, Ohli J, Elges S, Hartmann W, Klöppel G, Knösel T, Schulte M, Klein-Hitpass L, Beisser D, Reis H, Eyking A, Cario E, Schulte JH, Schramm A, Schüller U. Characterization of pancreatic glucagon-producing tumors and pituitary gland tumors in transgenic mice overexpressing MYCN in hGFAP-positive cells. *Oncotarget* 2016;7:74415–74426.
 17. Marino S, Vooijs M, van Der Gulden H, Jonkers J, Berns A. Induction of medulloblastomas in p53-null mutant mice by somatic inactivation of Rb in the external granular layer cells of the cerebellum. *Genes Dev* 2000;14:994–1004.
 18. Zhuo L, Theis M, Alvarez-Maya I, Brenner M, Willecke K, Messing A. hGFAP-cre transgenic mice for manipulation of glial and neuronal function in vivo. *Genesis* 2001;31:85–94.
 19. Wang Z, Ocadiz-Ruiz R, Sundaresan S, Ding L, Hayes M, Sahoo N, Xu H, Merchant JL. Isolation of enteric glial cells from the submucosa and lamina propria of the adult mouse. *J Vis Exp* 2018:57629.
 20. Mucke L, Oldstone MB, Morris JC, Nerenberg MI. Rapid activation of astrocyte-specific expression of GFAP-lacZ transgene by focal injury. *New Biol* 1991;3:465–474.
 21. Yachnis AT, Rorke LB, Lee VM, Trojanowski JQ. Expression of neuronal and glial polypeptides during histogenesis of the human cerebellar cortex including observations on the dentate nucleus. *J Comp Neurol* 1993;334:356–369.
 22. Johansson CB, Momba S, Clarke DL, Risling M, Lendahl U, Frisén J. Identification of a neural stem cell in the adult mammalian central nervous system. *Cell* 1999;96:25–34.
 23. Petri A, Ahnfelt-Rønne J, Frederiksen KS, Edwards DG, Madsen D, Serup P, Fleckner J, Heller RS. The effect of neurogenin3 deficiency on pancreatic gene expression in embryonic mice. *J Mol Endocrinol* 2006;37:301–316.
 24. Tang LH, Untch BR, Reidy DL, O'Reilly E, Dhall D, Jih L, Basturk O, Allen PJ, Klimstra DS. Well-differentiated neuroendocrine tumors with a morphologically apparent high-grade component: a pathway distinct from poorly differentiated neuroendocrine carcinomas. *Clin Cancer Res* 2016;22:1011–1017.
 25. Fang JM, Shi J. A Clinicopathologic and molecular update of pancreatic neuroendocrine neoplasms with a focus on the new World Health Organization Classification. *Arch Pathol Lab Med* 2019;143:1317–1326.
 26. Bellizzi AM. Immunohistochemistry in the diagnosis and classification of neuroendocrine neoplasms: what can brown do for you? *Hum Pathol* 2020;96:8–33.
 27. Vergès B, Boureille F, Goudet P, Murat A, Beckers A, Sassolas G, Cougard P, Chambe B, Montvernay C, Calender A. Pituitary disease in MEN type 1 (MEN1): data from the France-Belgium MEN1 multicenter study. *J Clin Endocrinol Metab* 2002;87:457–465.
 28. Goudet P, Bonithon-Kopp C, Murat A, Ruszniewski P, Niccoli P, Ménégau F, Chabrier G, Borson-Chazot F, Tabarin A, Bouchard P, Cadiot G, Beckers A, Guilhem I, Chabre O, Caron P, Du Boullay H, Verges B, Cardot-Bauters C. Gender-related differences in MEN1 lesion occurrence and diagnosis: a cohort study of 734 cases from the Groupe d'étude des Tumeurs Endocrines. *Eur J Endocrinol* 2011;165:97–105.
 29. Regoli M, Orazioli D, Gerli R, Bertelli E. Glial fibrillary acidic protein (GFAP)-like immunoreactivity in rat endocrine pancreas. *J Histochem Cytochem* 2000;48:259–266.
 30. Middeldorp J, Hol EM. GFAP in health and disease. *Prog Neurobiol* 2011;93:421–443.
 31. Zhang S, Cui Y, Ma X, Yong J, Yan L, Yang M, Ren J, Tang F, Wen L, Qiao J. Single-cell transcriptomics identifies divergent developmental lineage trajectories during human pituitary development. *Nat Commun* 2020;11:5275.
 32. Syro LV, Scheithauer BW, Kovacs K, Toledo RA, Londoño FJ, Ortiz LD, Rotondo F, Horvath E, Uribe H. Pituitary tumors in patients with MEN1 syndrome. *Clinics (Sao Paulo)* 2012;67(Suppl 1):43–48.
 33. Cohen-Cohen S, Brown DA, Himes BT, Wheeler LP, Ruff MW, Major BT, Singh Ospina NM, Atkinson JLD, Meyer FB, Bancos I, Young WF, Van Gompel JJ. Pituitary adenomas in the setting of multiple endocrine neoplasia type 1: a single-institution experience. *J Neurosurg* 2020;134:1132–1138.
 34. van den Berge SA, Middeldorp J, Zhang CE, Curtis MA, Leonard BW, Mastroeni D, Voorn P, van de Berg WD, Huitinga I, Hol EM. Longterm quiescent cells in the aged human subventricular neurogenic system specifically express GFAP-delta. *Aging Cell* 2010;9:313–326.
 35. Liu Y, Namba T, Liu J, Suzuki R, Shioda S, Seki T. Glial fibrillary acidic protein-expressing neural progenitors give rise to immature neurons via early intermediate progenitors expressing both glial fibrillary acidic protein and neuronal markers in the adult hippocampus. *Neuroscience* 2010;166:241–251.
 36. Raponi E, Agenes F, Delphin C, Assard N, Baudier J, Legraverend C, Deloulme JC. S100B expression defines a state in which GFAP-expressing cells lose their neural

- stem cell potential and acquire a more mature developmental stage. *Glia* 2007;55:165–177.
37. Lopez-Egido J, Cunningham J, Berg M, Oberg K, Bongcam-Rudloff E, Gobl A. Menin's interaction with glial fibrillary acidic protein and vimentin suggests a role for the intermediate filament network in regulating menin activity. *Exp Cell Res* 2002;278:175–183.
 38. Poisson A, Zablewska B, Gaudray P. Menin interacting proteins as clues toward the understanding of multiple endocrine neoplasia type 1. *Cancer Lett* 2003;189:1–10.
 39. Xiao C, Ogle SA, Schumacher MA, Orr-Asman MA, Miller ML, Lertkowitz N, Varro A, Hollande F, Zavros Y. Loss of parietal cell expression of Sonic hedgehog induces hypergastrinemia and hyperproliferation of surface mucous cells. *Gastroenterology* 2010;138:550–561.e1–8.
 40. Shirai N, Choudhary S, Houle C. Gastric neuroendocrine tumors with parietal cell atrophy in a long-term carcinogenicity study in rats. *Toxicol Pathol* 2022;50:507–511.
 41. Costa M, Furness JB, Yanaihara N, Yanaihara C, Moody TW. Distribution and projections of neurons with immunoreactivity for both gastrin-releasing peptide and bombesin in the guinea-pig small intestine. *Cell Tissue Res* 1984;235:285–293.
 42. Dutton R, Yamada T, Turnley A, Bartlett PF, Murphy M. Sonic hedgehog promotes neuronal differentiation of murine spinal cord precursors and collaborates with neurotrophin 3 to induce Islet-1. *J Neurosci* 1999;19:2601–2608.
 43. Villavicencio EH, Walterhouse DO, Iannaccone PM. The sonic hedgehog-patched-gli pathway in human development and disease. *Am J Hum Genet* 2000;67:1047–1054.
 44. Ding L, Sontz EA, Saqui-Salces M, Merchant JL. Interleukin-1 β suppresses gastrin via primary cilia and induces antral hyperplasia. *Cell Mol Gastroenterol Hepatol* 2021;11:1251–1266.
 45. Imura T, Kornblum HI, Sofroniew MV. The predominant neural stem cell isolated from postnatal and adult forebrain but not early embryonic forebrain expresses GFAP. *J Neurosci* 2003;23:2824–2832.
 46. Britsch S, Goerich DE, Riethmacher D, Peirano RI, Rossner M, Nave KA, Birchmeier C, Wegner M. The transcription factor Sox10 is a key regulator of peripheral glial development. *Genes Dev* 2001;15:66–78.
 47. Priestley P, Baber J, Lolkema MP, Steeghs N, de Bruijn E, Shale C, Duyvesteyn K, Haidari S, van Hoeck A, Onstenk W, Roepman P, Voda M, Bloemendal HJ, Tjan-Heijnen VCG, van Herpen CML, Labots M, Witteveen PO, Smit EF, Sleijfer S, Voest EE, Cuppen E. Pan-cancer whole-genome analyses of metastatic solid tumours. *Nature* 2019;575:210–216.
 48. Shen HC, He M, Powell A, Adem A, Lorang D, Heller C, Grover AC, Ylaya K, Hewitt SM, Marx SJ, Spiegel AM, Libutti SK. Recapitulation of pancreatic neuroendocrine tumors in human multiple endocrine neoplasia type 1 syndrome via Pdx1-directed inactivation of Men1. *Cancer Res* 2009;69:1858–1866.
 49. Shen HC, Ylaya K, Pechhold K, Wilson A, Adem A, Hewitt SM, Libutti SK. Multiple endocrine neoplasia type 1 deletion in pancreatic alpha-cells leads to development of insulinomas in mice. *Endocrinology* 2010;151:4024–4030.
 50. Wong C, Tang LH, Davidson C, Vosburgh E, Chen W, Foran DJ, Notterman DA, Levine AJ, Xu EY. Two well-differentiated pancreatic neuroendocrine tumor mouse models. *Cell Death Differ* 2020;27:269–283.
 51. Lines KE, Vas Nunes RP, Frost M, Yates CJ, Stevenson M, Thakker RV. A MEN1 pancreatic neuroendocrine tumour mouse model under temporal control. *Endocr Connect* 2017;6:232–242.
 52. Harding B, Lemos MC, Reed AA, Walls GV, Jeyabalan J, Bowl MR, Tateossian H, Sullivan N, Hough T, Fraser WD, Ansorge O, Cheeseman MT, Thakker RV. Multiple endocrine neoplasia type 1 knockout mice develop parathyroid, pancreatic, pituitary and adrenal tumours with hypercalcaemia, hypophosphataemia and hypercorticotesteronaemia. *Endocr Relat Cancer* 2009;16:1313–1327.
 53. Molofsky AV, Glasgow SM, Chaboub LS, Tsai HH, Murnen AT, Kelley KW, Fancy SP, Yuen TJ, Madireddy L, Baranzini S, Deneen B, Rowitch DH, Oldham MC. Expression profiling of Aldh1l1-precursors in the developing spinal cord reveals glial lineage-specific genes and direct Sox9-Nfe2l1 interactions. *Glia* 2013;61:1518–1532.
 54. Kaczmarczyk L, Reichenbach N, Blank N, Jonson M, Dittrich L, Petzold GC, Jackson WS. Slc1a3-2A-CreERT2 mice reveal unique features of Bergmann glia and augment a growing collection of Cre drivers and effectors in the 129S4 genetic background. *Sci Rep* 2021;11:5412.
 55. Tiwari N, Pataskar A, Péron S, Thakurela S, Sahu SK, Figueres-Oñate M, Marichal N, López-Mascaraque L, Tiwari VK, Berninger B. Stage-specific transcription factors drive astroglialogenesis by remodeling gene regulatory landscapes. *Cell Stem Cell* 2018;23:557–571, e8.
 56. Weng Q, Wang J, Wang J, He D, Cheng Z, Zhang F, Verma R, Xu L, Dong X, Liao Y, He X, Potter A, Zhang L, Zhao C, Xin M, Zhou Q, Aronow BJ, Blackshear PJ, Rich JN, He Q, Zhou W, Suvà ML, Waclaw RR, Potter SS, Yu G, Lu QR. Single-cell transcriptomics uncovers glial progenitor diversity and cell fate determinants during development and gliomagenesis. *Cell Stem Cell* 2019;24:707–723.e8.
 57. Chen KS, Bridges CR, Lynton Z, Lim JWC, Stringer BW, Rajagopal R, Wong KT, Ganesan D, Ariffin H, Day BW, Richards LJ, Bunt J. Transcription factors NFIA and NFIB induce cellular differentiation in high-grade astrocytoma. *J Neurooncol* 2020;146:41–53.
 58. Lam M, Sanosaka T, Lundin A, Imaizumi K, Etal D, Karlsson FH, Clausen M, Cairns J, Hicks R, Kohyama J, Kele M, Okano H, Falk A. Single-cell study of neural stem cells derived from human iPSCs reveals distinct progenitor populations with neurogenic and gliogenic potential. *Genes Cells* 2019;24:836–847.
 59. Bami M, Episkopou V, Gavalas A, Gouti M. Directed neural differentiation of mouse embryonic stem cells is a sensitive system for the identification of novel Hox gene effectors. *PLoS One* 2011;6:e20197.
 60. Gouti M, Gavalas A. Hoxb1 controls cell fate specification and proliferative capacity of neural stem and progenitor cells. *Stem Cells* 2008;26:1985–1997.

61. Gámez B, Rodríguez-Carballo E, Ventura F. BMP signaling in telencephalic neural cell specification and maturation. *Front Cell Neurosci* 2013;7:87.
62. Le Dréau G, Garcia-Campmany L, Rabadán MA, Ferronha T, Tozer S, Briscoe J, Martí E. Canonical BMP7 activity is required for the generation of discrete neuronal populations in the dorsal spinal cord. *Development* 2012;139:259–268.
63. Segklia A, Seuntjens E, Elkouris M, Tsalavos S, Stappers E, Mitsiadis TA, Huylebroeck D, Remboutsika E, Graf D. Bmp7 regulates the survival, proliferation, and neurogenic properties of neural progenitor cells during corticogenesis in the mouse. *PLoS One* 2012;7:e34088.
64. Voronova A, Fischer A, Ryan T, Al Madhoun A, Skerjanc IS. Ascl1/Mash1 is a novel target of Gli2 during Gli2-induced neurogenesis in P19 EC cells. *PLoS One* 2011;6:e19174.
65. Gurung B, Feng Z, Hua X. Menin directly represses Gli1 expression independent of canonical Hedgehog signaling. *Mol Cancer Res* 2013;11:1215–1222.
66. Gurung B, Feng Z, Iwamoto DV, Thiel A, Jin G, Fan CM, Ng JM, Curran T, Hua X. Menin epigenetically represses Hedgehog signaling in MEN1 tumor syndrome. *Cancer Res* 2013;73:2650–2658.
67. Boesmans W, Lasrado R, Vanden Berghe P, Pachnis V. Heterogeneity and phenotypic plasticity of glial cells in the mammalian enteric nervous system. *Glia* 2015;63:229–241.
68. McCallum S, Obata Y, Fourli E, Boeing S, Peddie CJ, Xu Q, Horswell S, Kelsh RN, Collinson L, Wilkinson D, Pin C, Pachnis V, Heanue TA. Enteric glia as a source of neural progenitors in adult zebrafish. *Elife* 2020;9:e56086.
69. Belkind-Gerson J, Graham HK, Reynolds J, Hotta R, Nagy N, Cheng L, Kamionek M, Shi HN, Aherne CM, Goldstein AM. Colitis promotes neuronal differentiation of Sox2+ and PLP1+ enteric cells. *Sci Rep* 2017;7:2525.
70. Verissimo CP, Carvalho JDS, da Silva FJM, Campanati L, Moura-Neto V, Coelho-Aguiar JM. Laminin and environmental cues act in the inhibition of the neuronal differentiation of enteric glia in vitro. *Front Neurosci* 2019;13:914.
71. Joseph NM, He S, Quintana E, Kim YG, Núñez G, Morrison SJ. Enteric glia are multipotent in culture but primarily form glia in the adult rodent gut. *J Clin Invest* 2011;121:3398–3411.
72. Barker N, van Es JH, Kuipers J, Kujala P, van den Born M, Cozijnsen M, Haegebarth A, Korving J, Begthel H, Peters PJ, Clevers H. Identification of stem cells in small intestine and colon by marker gene Lgr5. *Nature* 2007;449:1003–1007.
73. Rico K, Duan S, Pandey R, Chen Y, Chakrabarti J, Starr J, Zavros Y, Else T, Katona BW, Metz DC, Merchant JL. Genome analysis identifies differences in the transcriptional targets of duodenal versus pancreatic neuroendocrine tumors. *BMJ Open Gastroenterol* 2021;8:e000765.
74. Eicher AK, Kechele DO, Sundaram N, Berns HM, Poling HM, Haines LE, Sanchez JG, Kishimoto K, Krishnamurthy M, Han L, Zorn AM, Helmuth MA, Wells JM. Functional human gastrointestinal organoids can be engineered from three primary germ layers derived separately from pluripotent stem cells. *Cell Stem Cell* 2021;29:36–51.e6.
75. Pfaffl MW. A new mathematical model for relative quantification in real-time RT-PCR. *Nucleic Acids Res* 2001;29:e45.
76. Arocho A, Chen B, Ladanyi M, Pan Q. Validation of the 2-DeltaDeltaCt calculation as an alternate method of data analysis for quantitative PCR of BCR-ABL P210 transcripts. *Diagn Mol Pathol* 2006;15:56–61.

Received January 4, 2022. Accepted June 28, 2022.

Correspondence

Address correspondence to: Dr Juanita L. Merchant, University of Arizona, 1515 N. Campbell Ave, Tucson, AZ 85724. e-mail: jmerchant@arizona.edu; tel: (520) 626-7897; fax: (520) 626-1291.

CRedit Authorship Contributions

Suzann Duan, PhD (Conceptualization: Supporting; Data curation: Lead; Formal analysis: Lead; Methodology: Lead; Validation: Lead; Visualization: Lead; Writing – original draft: Lead; Writing – review & editing: Supporting)

Travis W. Sawyer, PhD (Data curation: Supporting; Formal analysis: Supporting; Software: Supporting)

Ricky A. Sontz, MS, BS (Methodology: Supporting; Validation: Supporting)

Bradley A. Wieland, BS (Data curation: Supporting)

Andres F. Diaz, MS, BS (Data curation: Supporting)

Juanita L. Merchant, MD, PhD (Conceptualization: Lead; Funding acquisition: Lead; Supervision: Lead; Writing – original draft: Supporting; Writing – review & editing: Lead)

Conflicts of interest

The authors disclose no conflicts.

Funding

This study was funded by National Institutes of Health Research Project grant R01 DK45729-27 to Juanita L. Merchant.